Cell Reports

Article

Mycobacterial infection aggravates *Helicobacter pylori*-induced gastric preneoplastic pathology by redirection of *de novo* induced Treg cells

Graphical abstract

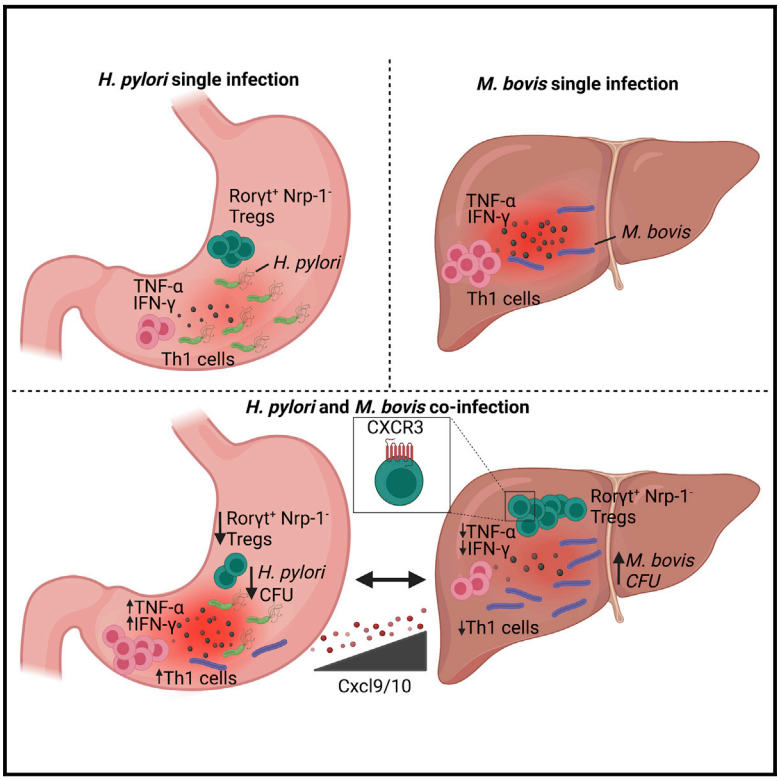

Highlights

- Co-infection of *M. bovis* and *H. pylori* boosts gastric Th1 responses and immunopathology
- Gastric presence of *H. pylori* compromises immune control of *M. bovis*
- Both mutual effects result from redirection of Treg cells to sites of *M. bovis* infection
- CXCR3 blockade restores *M. bovis* control, even if *H. pylori* is present

Authors

Mariela Artola-Borán, Angela Fallegger, Martina Priola, ..., Hans-Uwe Simon, Phil F. Cheng, Anne Müller

Correspondence

mueller@imcr.uzh.ch

In brief

Mtb and *Helicobacter pylori* are two common bacterial pathogens that overlap in many geographical areas of the world. Here, Artola-Borán et al. show in suitable mouse models how co-infection of *H. pylori* with the Mtb relative *M. bovis* affects immune responses to, and immunopathology associated with, both pathogens.

Artola-Borán et al., 2022, Cell Reports *38*, 110359
February 8, 2022
https://doi.org/10.1016/j.celrep.2022.110359

CellPress

Cell Reports

CellPress
OPEN ACCESS

Article

Mycobacterial infection aggravates *Helicobacter pylori*-induced gastric preneoplastic pathology by redirection of *de novo* induced Treg cells

Mariela Artola-Borán,[1,9] Angela Fallegger,[1,9] Martina Priola,[1] Rima Jeske,[2] Tim Waterboer,[2] Anders B. Dohlman,[3] Xiling Shen,[3] Sebastian Wild,[1] Jiazhuo He,[1] Mitchell P. Levesque,[4] Shida Yousefi,[5] Hans-Uwe Simon,[5,6,7,8] Phil F. Cheng,[4] and Anne Müller[1,10,*]

[1]Institute of Molecular Cancer Research, University of Zurich, Zurich, Switzerland
[2]Infection and Cancer Epidemiology, German Cancer Research Center, Heidelberg, Germany
[3]Department of Biomedical Engineering, Center for Genomics and Computational Biology, Duke Microbiome Center, Duke University, Durham, NC, USA
[4]Department of Dermatology, University Hospital Zurich, Zurich, Switzerland
[5]Institute of Pharmacology, University of Bern, Bern, Switzerland
[6]Department of Clinical Immunology and Allergology, Sechenov University, Moscow, Russia
[7]Laboratory of Molecular Immunology, Institute of Fundamental Medicine and Biology, Kazan Federal University, Kazan, Russia
[8]Institute of Biochemistry, Medical School Brandenburg, Neuruppin, Germany
[9]These authors contributed equally
[10]Lead contact
*Correspondence: mueller@imcr.uzh.ch
https://doi.org/10.1016/j.celrep.2022.110359

SUMMARY

The two human pathogens *Helicobacter pylori* and *Mycobacterium tuberculosis* (Mtb) co-exist in many geographical areas of the world. Here, using a co-infection model of *H. pylori* and the Mtb relative *M. bovis* bacillus Calmette-Guérin (BCG), we show that both bacteria affect the colonization and immune control of the respective other pathogen. Co-occurring *M. bovis* boosts gastric Th1 responses and *H. pylori* control and aggravates gastric immunopathology. *H. pylori* in the stomach compromises immune control of *M. bovis* in the liver and spleen. Prior antibiotic *H. pylori* eradication or *M. bovis*-specific immunization reverses the effects of *H. pylori*. Mechanistically, the mutual effects can be attributed to the redirection of regulatory T cells (Treg cells) to sites of *M. bovis* infection. Reversal of Treg cell redirection by CXCR3 blockade restores *M. bovis* control. In conclusion, the simultaneous presence of both pathogens exacerbates the problems associated with each individual infection alone and should possibly be factored into treatment decisions.

INTRODUCTION

Mycobacterium tuberculosis (Mtb) and *Helicobacter pylori* (*H. pylori*) are two of the most common bacterial pathogens chronically infecting humans, with one-half of the world's population being infected with *H. pylori* (Hooi et al., 2017) and approximately one-quarter infected with Mtb (Horsburgh and Rubin, 2011; Houben and Dodd, 2016). Of the latter, 5%–15% will develop active tuberculosis over their lifetime (Horsburgh and Rubin, 2011). Roughly 1%–3% of *H. pylori*-infected individuals will develop gastric cancer, for which *H. pylori* is a major risk factor (Parsonnet et al., 1991; Uemura et al., 2001); the vast majority (80%–90%) of *H. pylori* carriers remain asymptomatic throughout their lifetime (Peek and Blaser, 2002). Additional gastric cancer risk factors include a diet high in sodium chloride and low in vitamin C, smoking, obesity, and genetic determinants affecting the expression of pro-inflammatory cytokines, such as interleukin-1β , its receptor, and others (Crabtree and Wessler, 2018; Yusefi et al., 2018). Epstein-Barr virus (EBV) is a known infectious risk factor of gastric cancer (Bae and Kim, 2016), but bacteria other than *H. pylori* have not been implicated in gastric cancer development, neither in epidemiological studies nor in experimental models. As Mtb and *Helicobacter pylori* are extremely common, both pathogens are likely to co-exist in a substantial proportion of their human hosts. Geographical areas of the world where both pathogens are highly prevalent (>20% for Mtb; >50% for *H. pylori*) include Eastern Europe, Russia, China, South and South-East Asia, and South America; in contrast, both pathogens are comparatively underrepresented in Western Europe, North America, and Australia (Figures S1A and S1B; Houben and Dodd, 2016; Zamani et al., 2018). Mortality from gastric cancer is highest in Russia, China, and parts of South America (Rawla and Barsouk, 2019). Eastern European countries, Russia, and China in particular are afflicted by high rates of active tuberculosis and tuberculosis-associated mortality and also suffer from extremely high gastric cancer mortality rates (Figures S1C and S1D).

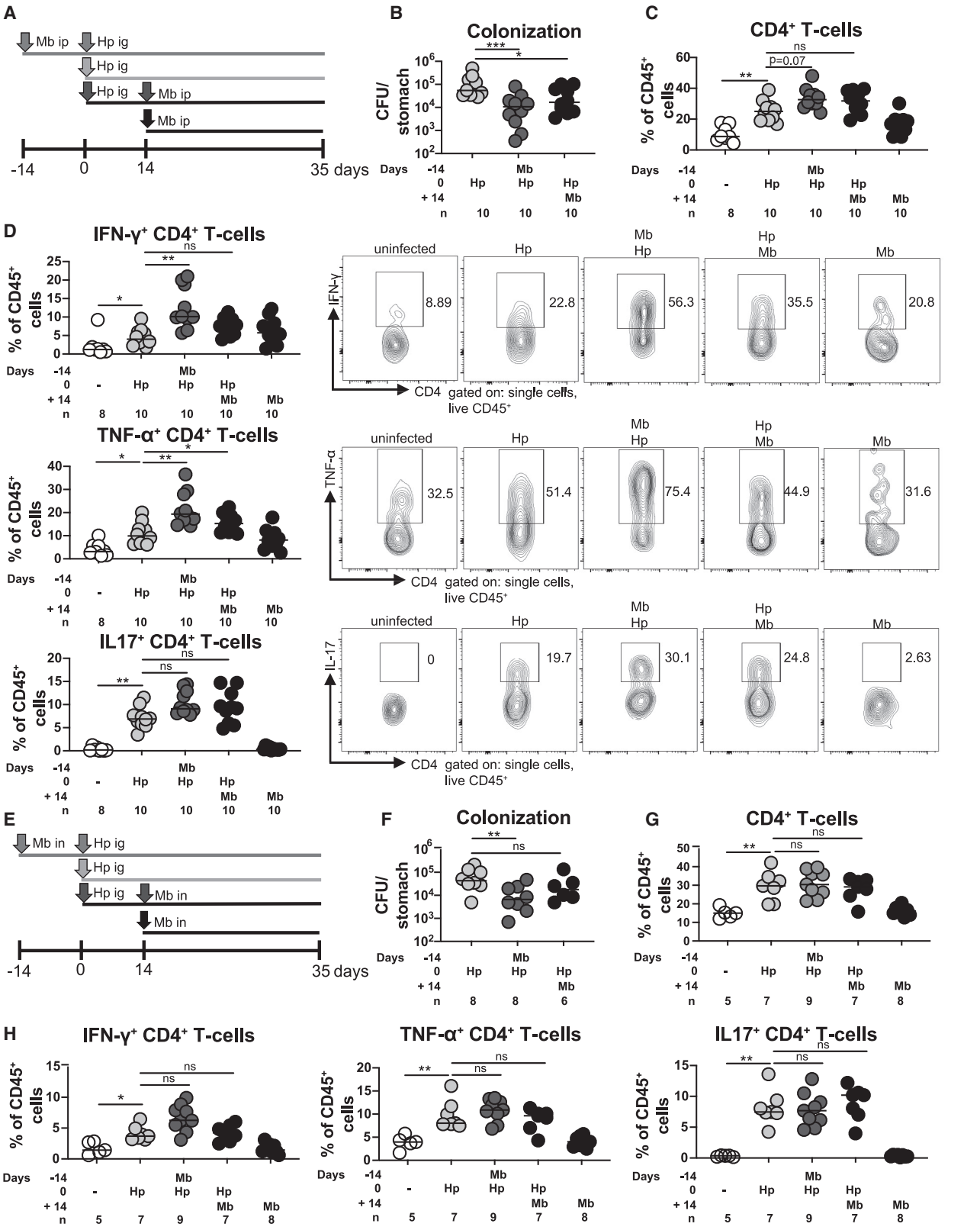

(legend on next page)

Experimental mouse models are available to study the immune responses to and pathology associated with mycobacterial and *H. pylori* infection. *M. bovis* bacillus Calmette-Guérin (BCG) infection of C57BL/6 mice mimics many aspects of Mtb infection in humans, such as Mtb chronicity, the induction of granulomas, the pronounced Th1 polarization of anti-mycobacterial T cell responses, and the tropism for the lung as well as certain systemic sites (liver and spleen; Arnold et al., 2019; Erb et al., 1998; Saxena et al., 2002; Zhang et al., 2020). Infection of C57BL/6 mice with a mouse-colonizing patient isolate of *H. pylori*, strain PMSS1, recapitulates the chronic gastritis; mixed Th1/Th17 response; and, upon long-term exposure, development of gastric preneoplastic lesions, such as atrophic gastritis, epithelial hyperplasia, and intestinal metaplasia, that are characteristic of non-asymptomatic human carriers of *H. pylori* (Arnold et al., 2011a). We combined the two models and found that both pathogens profoundly affect immunity—and the associated immunopathology—to the other infectious agent and were able to attribute the mutual interaction to a strong redirection of regulatory T cells. In co-infected mice, this re-routing of regulatory T cells (Treg cells) toward sites of *M. bovis* colonization results in a pronounced failure of the host to control *M. bovis* but permits unrestricted T cell control of *H. pylori*, the downside of the latter being more pronounced preneoplastic pathology.

RESULTS

M. bovis BCG improves *Helicobacter pylori* immune control by enhancing gastric T helper responses

To examine the effects of *M. bovis* BCG on various outcomes of gastric *H. pylori* infection, we intragastrically infected mice for 5 weeks with either *H. pylori* alone or in conjunction with intraperitoneally (i.p.) administered *M. bovis* BCG (see schematic in Figure 1A). i.p. administration of *M. bovis* results in both liver and spleen colonization and granulomatosis of the liver (Arnold et al., 2019; Zhang et al., 2020; Figure S1E). *M. bovis* was administered either 2 weeks before or after *H. pylori* (Figure 1A). Prior *M. bovis* infection resulted in significantly reduced *H. pylori* colonization (Figure 1B) and higher frequencies and absolute numbers of $CD4^+$ T cells and especially of interferon (IFN)-γ-, tumor necrosis factor alpha (TNF-α)-, and IL-17-producing $CD4^+$ T cells in the infected gastric mucosa (Figures 1C, 1D, and S1F); CD8 T cell responses did not differ as a consequence of co-infection with *M. bovis* (data not shown). *M. bovis* administration after *H. pylori* infection had less pronounced effects on *H. pylori* colonization levels and the T cell compartment than prior *M. bovis* administration (Figures 1B–1D and S1F). Transcript levels of T cell cytokines confirmed the general trends obtained by intracellular cytokine staining, although later *M. bovis* infection had stronger effects on cytokines than prior *M. bovis* infection, according to this readout (Figure S1G); the reason for this discrepancy might be due to cytokine production by cells not captured by the lymphocyte markers included in our staining panel. Multiplex serology conducted on sera of single- or co-infected mice showed that antibodies to many of the dominant *H. pylori* antigens were more abundant in mice that had additionally been infected with *M. bovis* (Figure S1H). To investigate whether an alternative route of *M. bovis* administration would have similar consequences for *H. pylori*-specific gastric readouts, we infected mice intranasally (i.n.) with *M. bovis*, either before or after *H. pylori* administration (Figure 1E). i.n. administration of *M. bovis* results in lung colonization (Figure S1I) and the appearance of macrophage infiltrates in the lung (Figure S1E) that are, however, much less well organized than the granulomas found in the liver. i.n. delivery of *M. bovis* recapitulated the effects of systemic (i.p.) *M. bovis* BCG infection, with reduced *H. pylori* colonization, and enhanced Th1 responses observed with prior, but not later, administration of *M. bovis* (Figures 1F–1H and S1J). Th17 responses were less affected by *M. bovis* administration (Figures 1H and S1J). Interestingly, a substantial proportion of gastric $CD4^+$ T cells were BCG specific as determined by intracellular cytokine staining upon restimulation with *M. bovis* purified protein derivative (PPD), a mixture of *M. bovis*-derived protein components (Figure S1K). The combined data from both types of co-infection models (i.p. versus i.n. *M. bovis* administration) suggest that mycobacterial infection of the lung or of systemic sites, especially if it is established before the host is confronted with *H. pylori*, has profound effects on the host's ability to control this gastric pathogen. In the presence of *M. bovis*, *H. pylori* is controlled more effectively, and this can likely be attributed to an overshooting effector T cell response.

M. bovis aggravates *Helicobacter pylori*-associated gastric immunopathology

Gastric preneoplastic lesions form as a consequence of *H. pylori*-specific T cell responses; the most commonly observed lesions in

Figure 1. Co-infection with *M. bovis* BCG improves *Helicobacter pylori* immune control by enhancing gastric Th1 responses

(A) Schematic of the sequence of intraperitoneal (i.p.) *M. bovis* and intragastric (i.g.) *H. pylori* infection of the groups shown in (B)–(D).

(B) *H. pylori* colonization of single- and co-infected mice, represented as CFUs per stomach.

(C) Frequencies of gastric lamina propria $CD4^+$ T cells among all $CD45^+$ leukocytes.

(D) Frequencies of IFN-γ^+, TNF-α^+, and IL-17^+ $CD4^+$ T cells among all $CD45^+$ leukocytes as determined by intracellular cytokine staining upon PMA/ionomycin restimulation. Data in (B)–(D) are pooled from two independent studies.

(E) Schematic of the sequence of intranasal (i.n.) Mb and i.g. Hp infection of the groups shown in (F)–(I).

(F) *H. pylori* colonization of single- and co-infected mice, represented as CFUs per stomach.

(G) Frequencies of gastric lamina propria $CD4^+$ T cells among all $CD45^+$ leukocytes.

(H) Frequencies of IFN-γ^+, TNF-α^+, and IL-17^+ $CD4^+$ T cells among all $CD45^+$ leukocytes as determined by intracellular cytokine staining upon PMA/ionomycin restimulation. Data in (F)–(H) are all from one study. Note that a few mice of the study were lost to follow-up by fluorescence-activated cell sorting (FACS) due to cell viability issues.

Statistical comparisons in (B)–(D) and (F)–(H) were done by Kruskal-Wallis test followed by Dunn's post-hoc test. Only relevant (i.e., between single *H. pylori*- and co-infected mice or to uninfected controls) comparisons are shown. *$p < 0.05$, **$p < 0.01$, ***$p < 0.001$, ****$p < 0.0001$, and ns, not significant. n indicates the number of mice per group. See also Figure S1.

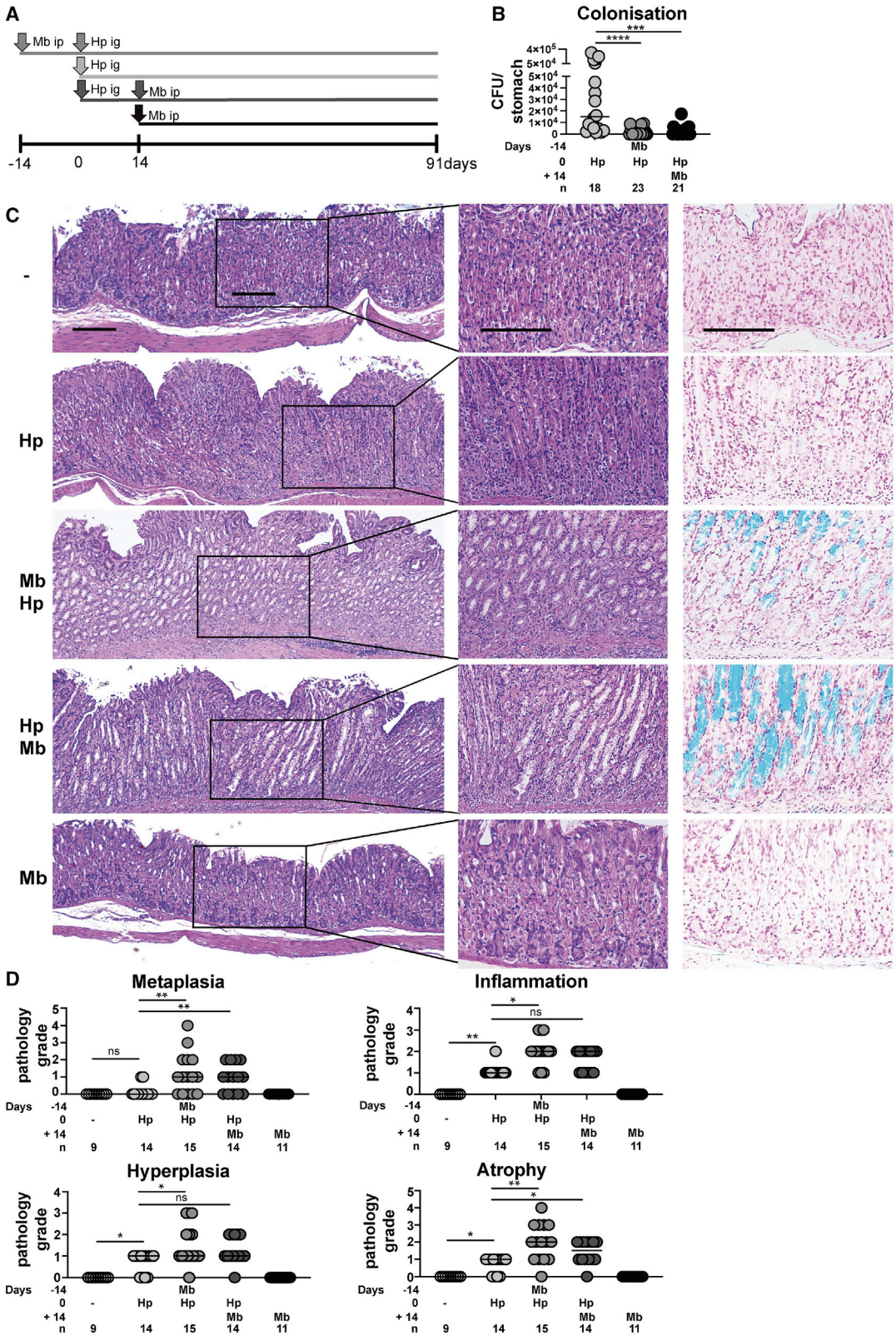

(legend on next page)

mice are chronic atrophic gastritis, epithelial hyperplasia resulting from the hyperproliferation of non-differentiated progenitor cells, and intestinal metaplasia, which represents the aberrant differentiation of gastric stem cells into intestinal goblet-cell-resembling cells (Arnold et al., 2011a). Such lesions typically arise within 3 months of infection and can readily be visualized by H&E staining as well as Alcian blue staining for intestinal metaplasia and Ki67 staining for hyperplasia (Arnold et al., 2011a; Sayi et al., 2009, 2011). To address whether the enhanced gastric Th1 responses of *M. bovis* and *H. pylori* co-infected mice result in more severe immunopathology, we infected mice with *H. pylori* for 3 months and administered *M. bovis* i.p. either 2 weeks before or after *H. pylori* (see schematic in Figure 2A). The colonization patterns of single- and co-infected mice recapitulated the patterns obtained after 5 weeks of *H. pylori* infection, with reduced *H. pylori* colonization observed in co-infected mice (Figure 2B). Reduced colonization levels were accompanied by and likely attributable to enhanced Th1 responses as judged by intracellular cytokine staining (frequencies and absolute numbers of IFN-γ- and TNF-α-expressing $CD4^+$ T cells) and qRT-PCR for Th1 signature transcripts (Figures S2A–S2D). Interestingly, co-infected mice developed on average more gastric pathology, i.e., more inflammation, hyperplasia, atrophy, and intestinal metaplasia, than *H. pylori* single-infected mice (Figures 2C and 2D). In particular, we observed widespread Alcian-blue-positive intestinal metaplasia and Ki67-positive epithelial hyperplasia, each affecting one-third or more of the corpus area, in the majority of co-infected mice, whereas these lesion were rare and limited to very few (up to three) glands in *H. pylori* single-infected mice (Figures 2C, 2D, and S2E). Similarly, the extent of gastric atrophy, i.e., the loss of specialized epithelial cells (parietal and chief cells), was more pronounced in co-infected mice, as was the degree of mucosal and submucosal inflammation (Figures 2C and 2D). Prior *M. bovis* infection resulted in somewhat more pathology and higher Th1 responses than later *M. bovis* infection; *M. bovis* alone did not trigger the formation of gastric preneoplastic lesions (Figures 2C and 2D). The combined results indicate that the dysregulated gastric T cell responses in the stomachs of co-infected mice result in more pronounced gastric immunopathology and premalignant lesions.

M. bovis colonizes the gastric mucosa and triggers a strong local effector T cell response

Having observed that a substantial proportion of gastric $CD4^+$ T cells could be restimulated with the *M. bovis* PPD protein mixture in mice that had been i.p. infected with *M. bovis* BCG—both with and without simultaneous presence of *H. pylori* (Figure S1K)—we asked whether *M. bovis* might be able to colonize the gastric mucosa. Indeed, plating of gastric homogenates on Middlebrock agar plates supporting *M. bovis* growth revealed colony-forming units in all infected, but not uninfected, mice (Figure S3A). The presence of *M. bovis* could be confirmed by quantitative PCR (qPCR) using *M. bovis*-specific primers (Lesellier et al., 2019), not only in the stomach (Figure 3A) but also in the small intestine and colon of the same mice (note that qPCR and colony-forming unit [CFU] data correlate very well; Figures S3B and S3C). A time course of 3, 5, and 10 weeks of *M. bovis* infection revealed that the presence of *M. bovis* in the stomach peaked at 5 weeks post-infection as judged by qPCR analyses (Figure 3A) and was further accompanied by a strong transcriptional Th1, but not Th17, signature, with upregulation of *Ifng* and its target genes *Cxcl9* and *Cxcl10*, as well as *Il12* and *Tnfa*, but not, *Il17* (Figure 3B). We chose the 5-week infection time point to flow cytometrically characterize in more detail the gastric $CD4^+$ T cell compartment upon single-pathogen infection with *M. bovis* or with *H. pylori*. Both pathogens induced a strong Th1 response, i.e., $CD4^+$ T cells that expressed IFN-γ or TNF-α; only *H. pylori* additionally induced Th17 cells expressing IL-17, whereas *M. bovis* additionally induced IL-10 production by $CD4^+$ T cells (Figures 3C and 3D). A further interesting difference was observed with respect to the multifunctionality of $CD4^+$ T cells. Whereas the dominant $CD4^+$ T cell populations in *H. pylori*-infected stomachs expressed either TNF-α, IL-17, or TNF-α in conjunction with IFN-γ (but not IL-10), the $CD4^+$ T cell populations of the *M. bovis*-infected stomachs were multifunctional, i.e., positive for IFN-γ, TNF-α, and IL-10 (but not IL-17; Figure 3E). The fact that different protocols were used for restimulation (phorbol myristate acetate [PMA]/ionomycin in the setting of *H. pylori* infection; PPD in the *M. bovis* setting) complicates the interpretation of these results; regardless of the procedure, however, cytokine-positive $CD4^+$ T cell populations were much less abundant in the naive gastric mucosa (Figures 3C–3E). *M. bovis*-infected mice showed absolutely no signs of gastric pathology as shown above (Figures 2C and 2D), and granulomas were not observed. In summary, it appears from single-infection settings that *M. bovis* is capable of establishing live infection in the stomach, which triggers a Th1 response characterized by multifunctional T cells that by itself is non-immunopathological and clearly distinct from the mixed Th1/Th17 response launched against *H. pylori* by the same tissue.

An Mtb signature is present in tumor and adjacent tissue of gastric cancer patients

Having obtained plausible experimental evidence for a contributing role of mycobacterial infection in gastric carcinogenesis,

Figure 2. *M. bovis* co-infection aggravates *H. pylori*-associated gastric immunopathology upon long-term exposure to both pathogens

(A) Schematic of the sequence of i.p. *M. bovis* and i.g. *H. pylori* infection of the groups shown in (B)–(D).

(B) *H. pylori* colonization of single- and co-infected mice, represented as CFUs per stomach.

(C) Representative H&E-stained images of mice of the indicated treatment groups, at low (10×, left) and high (20×, inset) magnification. Alcian-blue-stained images of the same high magnification area are shown in the right panels. Scale bars, 100 μm.

(D) Scores as assigned to each mouse per group, on a scale of 0–6 according to the updated Sydney classification, of the four parameters intestinal metaplasia, chronic inflammation, epithelial hyperplasia, and gastric atrophy. Data in (B) are pooled from three studies; data in (C) and (D) are from two of the three studies; and material from the second 3-month infection study was used for leukocyte preparation and T cell restimulation (see Figure S2).

Statistical comparisons in (B) and (D) were done by Kruskal-Wallis test followed by Dunn's post-hoc test. Only relevant (i.e., between single *H. pylori*- and co-infected mice) comparisons are shown. $^{**}p < 0.01$, $^{***}p < 0.001$, and $^{****}p < 0.0001$. n indicates the number of mice per group. See also Figure S2.

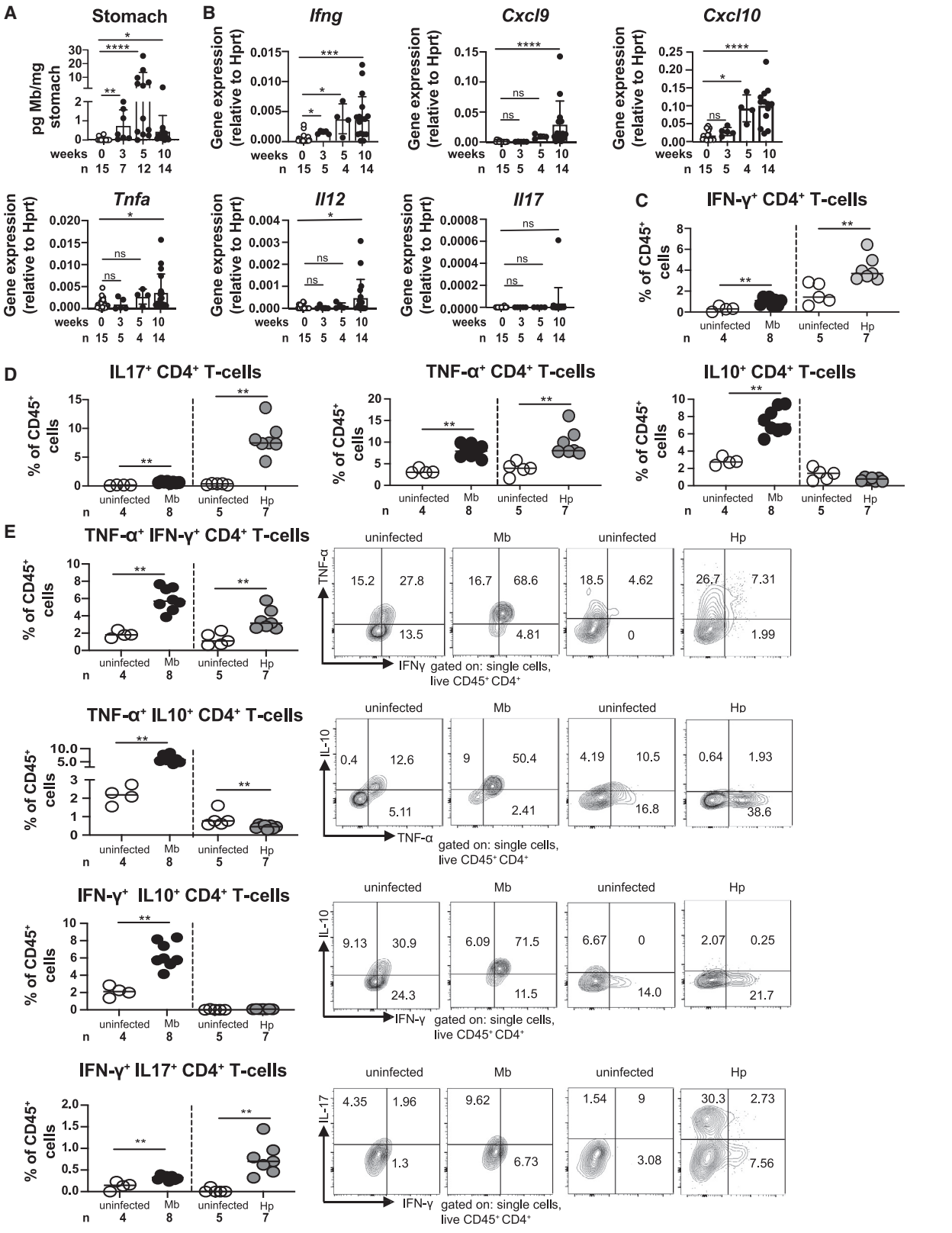

(legend on next page)

we queried whole-exome sequencing data from 291 gastric cancer patients for whom both tumor and adjacent normal sequences were available through the Cancer Genome Atlas (TCGA) consortium. Previous analysis of this dataset revealed four distinct molecular profiles: tumors positive for EBV; microsatellite unstable (MSI) tumors; genomically stable (GS) tumors; and tumors with chromosomal instability (CIN) (Bass et al., 2014). Presence of *H. pylori* and Mtb DNA was determined using data from The Cancer Microbiome Atlas (TCMA) (Dohlman et al., 2021). Of the 291 cases, 72 (i.e., 25%) exhibited evidence of the presence of *H. pylori* and 53 (18%) showed evidence of Mtb (Figure 4A). Forty-two cases (14%) were positive for both bacteria, and 124 cases (43%) were negative for both species (Figure 4A). Out of the four molecular subtypes, MSI subtype had the highest and the EBV-positive subtype had the lowest rates of *M. tuberculosis* positivity (Figure 4A). In patients with positive *H. pylori* status, *H. pylori* reads were ~300 times and significantly ($p = 2 \times 10^{-5}$) more abundant in normal adjacent tissue compared with tumor; this was not the case for Mtb, which was equally represented in normal relative to tumor tissue (Figure 4B). There were more reads to be found for *H. pylori* than for Mtb in both tumor (approximately six times; $p = 3.2 \times 10^{-12}$) and normal tissue (~7,300 times, $p = 2 \times 10^{-9}$; Figure 4B). In the general US population, positive tuberculin skin and IFN-γ release tests have led to estimates of around 5% Mtb prevalence, which have not changed substantially in the last 30 years (Miramontes et al., 2015); the prevalence of Mtb thus appears to be higher in the gastric cancer patient than in the general US reference population. Within subtypes, which differed substantially in their tumor mutational burden, cancers of Mtb-"positive" patients had a similar mutational burden than cancers of Mtb-negative patients (Figure S4A). Similarly, within each subtype, the top 50 most recurrently mutated genes did not segregate Mtb-positive and -negative cases (Figure S4B), transcriptional profiles were not different between Mtb-positive and -negative cases (Figure S4C), and CIBERSORT analysis did not suggest differential infiltration of Mtb-positive versus -negative cases with any of the 22 leukocyte populations that can be identified via their transcriptional signature using this method (Chen et al., 2018; Figure S4D). However, 79 genes were differentially and significantly ($p < 0.05$ according to Fisher's exact test) mutated in Mtb-positive, but not -negative, cases in one or more of the genetic subtypes of gastric cancer (Figure S4E), which points to a genetic signature of Mtb-associated cases. Our annotation of gastric cancer cases with their Mtb status and subsequent bioinformatic mining of genetic and transcriptional data lends circumstantial support to our observation that gastric preneoplasia is aggravated by mycobacterial infection in an experimental model.

H. pylori presence in the stomach compromises immunity to *M. bovis*, which is not properly controlled in a co-infection

To assess the effects of *H. pylori* infection on anti-mycobacterial immunity, we infected mice with *M. bovis* i.p. for a duration of 4 weeks in total, which was either preceded or not by intragastrically administered *H. pylori* (Figure 5A). Interestingly, more colonies of *M. bovis* were retrieved by plating and colony counting of both the spleen and the liver of mice that were co-infected with *H. pylori*, relative to mice that were infected with *M. bovis* only (Figure 5B), and these patterns could be confirmed by DNA-based quantification of *M. bovis* infection (Figure 5C). As *M. bovis* in the liver resides within granulomas (Arnold et al., 2019; Zhang et al., 2020), and the number of granulomas is directly proportional to the presence of *M. bovis* DNA in the liver (Figure S5A), we set out to quantify liver granulomas in single- and co-infected mice. Indeed, the livers of *M. bovis*-infected mice harbored many more granulomas if *H. pylori* was additionally present in the stomach (Figure 5D). The frequencies of *M. bovis*-specific hepatic Th1 cells expressing IFN-γ or TNF-α were reduced if *H. pylori* was present in the stomach, providing a likely explanation for the impaired clearance of *M. bovis* by co-infected mice (Figure 5E). Several Th1 cytokines or their downstream targets (*Csf2*, *Cxcl10*, *Ifng*, and *Il12*) were reduced at the transcript level in livers of co-infected relative to BCG-single-infected mice (Figure S5B); the Th17 cytokines IL-17 and IL-23 were not elevated in either single- or co-infected mice (Figure S5B). *H. pylori* eradication by 2 weeks of daily administration of the antibiotics metronidazole and tetracycline together with bismuth, a cocktail also used in humans to eliminate *H. pylori*, was not only successful at completely clearing the *H. pylori* infection (data not shown; no colonies detected on any of the plates) but also restored immune control of *M. bovis* BCG, as evidenced by its reduced colonization of the spleen and liver (Figures 5F and 5G). We next asked whether the effects of prior subcutaneous immunization with live *M. bovis* (mimicking the

Figure 3. Live *M. bovis* can be detected in and isolated from the murine gastric mucosa and triggers a local, multifunctional $CD4^+$ T cell response

(A) Gastric *M. bovis* colonization as detected and quantified (in pg DNA/mg of tissue) by qPCR using genomic DNA as template of mice that were i.p. infected with *M. bovis* for 3, 5, or 10 weeks.

(B) Transcript levels of the indicated cytokines as assessed by qRT-PCR of scraped gastric mucosa of the mice shown in (A). Gene expression is normalized to the housekeeping gene *Hprt*. Means ± SD are shown alongside individual symbols for all mice of the study. Note that not all mice were available for follow-up in both readouts.

(C and D) Frequencies of IFN-γ^+, TNF-α^+, IL-17^+, and IL-10^+ $CD4^+$ T cells among all $CD45^+$ leukocytes as determined by intracellular cytokine staining upon PPD-specific restimulation (*M. bovis*) or upon PMA/ionomycin restimulation (*H. pylori*) of mice that were infected for 5 weeks with either one or the other bacterium (i.p. for *M. bovis* and i.g. for *H. pylori*) or remained uninfected.

(E) Frequencies of the indicated bifunctional $CD4^+$ T cells among all $CD45^+$ leukocytes of the mice shown in (C) and (D); representative contour plots of the $CD4^+$ T cell compartment are shown alongside summary plots of all mice of the study.

Data in (A)–(E) are from a total of three studies, one of which was used for leukocyte preparation (5-week time point) and two of which (all three time points) were used for qPCR and qRT-PCR, respectively. Statistical comparisons were done by Kruskal-Wallis in (A) and (B) and by Mann-Whitney test in (C)–(E). Only relevant comparisons are shown. *$p < 0.05$, **$p < 0.01$, ***$p < 0.001$, and ****$p < 0.0001$. n indicates the number of mice per group. See also Figure S3.

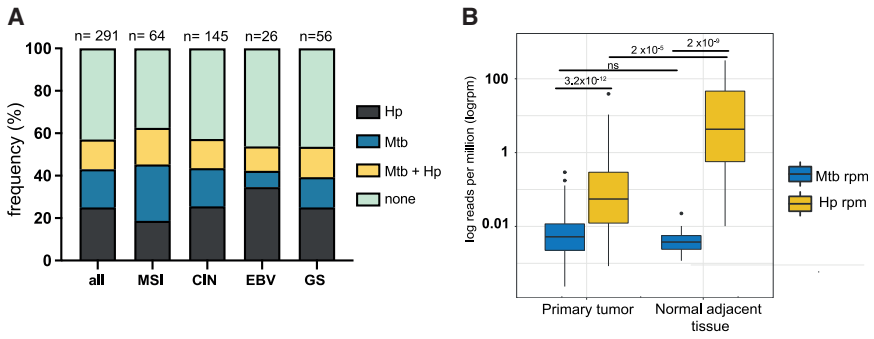

Figure 4. *Mycobacterium tuberculosis* (Mtb) DNA is present in gastric cancer biopsies, both with and without evidence of co-occurring *H. pylori* infection

(A) Mtb and *H. pylori* status of 291 gastric cancers available through TCGA, stratified by genetic subtype. CIN, chromosomally unstable subtype; EBV, Epstein-Barr virus-positive subtype; GS, genomically stable subtype; MSI, microsatellite unstable subtype.

(B) Reads per million, log-transformed, of Mtb and *H. pylori* in whole-exome sequencing data of 291 tumor versus 82 adjacent normal tissues of gastric cancer patients. Statistical comparisons were performed using the Student's t test.

See also Figure S4.

intradermal immunization with live bacteria that represents the mainstay of tuberculosis prevention in parts of the world in which Mtb remains endemic) on *M. bovis* immune control would also be compromised by the gastric presence of *H. pylori*. To that end, we immunized mice with a single subcutaneous dose of 1 million *M. bovis* BCG prior to i.p. single or co-challenge infection with live *M. bovis* and *H. pylori* (Figure 5H). Prior immunization reduced the elevated *M. bovis* colonization of co-infected mice to levels more characteristic of *M. bovis* mono-infection (Figure 5I). The combined data suggest that the presence of *H. pylori* in the gastric mucosa compromises immune control of *M. bovis* at systemic sites; these effects are neutralized by prior *M. bovis*-specific immunization and require a persistent and active *H. pylori* infection, as eradication of *H. pylori* restores immune control.

Gastrointestinally generated regulatory T cells are redirected to the *M. bovis*-infected liver, compromising *M. bovis* control on the one hand and boosting *H. pylori* control on the other

We hypothesized that a redirection of Treg cells from the stomach-draining lymph nodes to the liver might best explain the observed simultaneous improved clearance of *H. pylori* in the stomach and impaired clearance of *M. bovis* in the liver of co-infected mice. To examine this possibility, we profiled the Treg cell compartment in the liver and stomach of single- and co-infected animals (see schematic in Figure 6A). *H. pylori* is known to induce an abundant population of *de novo* generated, neuropilin-negative (Nrp-1$^-$), RORγt- and Tbet-expressing Treg cells that are primed in the draining lymph nodes and subsequently recruited to and expanded in the gastric lamina propria (Arnold et al., 2019). The frequencies and absolute counts of gastric Nrp-1$^+$ Treg cells, in contrast, are not affected by *H. pylori* infection (Arnold et al., 2019). Nrp-1$^+$ Treg cells originate in the thymus and are mainly tasked with suppressing autoimmunity, whereas Nrp-1$^-$ Treg cells are generated extrathymically in peripheral tissues and believed to suppress inappropriate immune responses to foreign antigens (Savage et al., 2020). Whereas *de novo* induced Nrp-1$^-$ Foxp3$^+$ Treg cells were readily detected in the gastric mucosa of *H. pylori*-infected mice also in this study, we found their frequencies to be strongly reduced in the setting of *H. pylori* and *M. bovis* co-infection (Figure 6B). The strongest differences resulting from single *H. pylori* and from *H. pylori* and *M. bovis* co-infection were observed in the RORγt$^+$ Nrp-1$^-$ Treg cell population (Figures 6C and 6D), which in the infected gastric lamina propria is also positive for Tbet (Figure 6E). RORγt$^-$ Nrp-1$^-$ Treg cells were not affected by single or co-infection (Figure S6A). To examine whether a putative redirection of *H. pylori*-induced Treg cells would manifest in differential Treg cell populations in the liver, we examined the hepatic Treg cell populations of the single- and co-infected mice shown in Figures 6B–6D. All *M. bovis*-infected mice showed an increase in Foxp3$^+$ Nrp-1$^-$ Treg cells relative to uninfected controls, irrespective of the simultaneous presence or absence of *H. pylori* (Figure 6F). Interestingly, mice that were co-infected with both bacterial species exhibited a hepatic RORγt$^+$ Nrp-1$^-$ Treg cell population; this population was not present in mice exposed only to *M. bovis* (Figures 6G and 6H). This population expressed both RORγt and Tbet (Figure 6I). RORγt-negative Nrp-1$^-$ Treg cells were induced by *M. bovis* but did not differ as a function of *H. pylori* co-infection (Figure 6G). Immunofluorescence staining of liver sections for Treg cells and macrophages revealed that Treg cells reside within liver granulomas in co-infected and *M. bovis*-only-infected mice (Figures 6J and S6B). Many more Treg cells were detected by automated cell counting of co-infected livers (1.06 ± 0.26 Treg cells/mm^2) than of uninfected (0.07 ± 0.017) or *M. bovis*-only livers (0.8 ± 0.4). Prior subcutaneous immunization with *M. bovis*, which overrides the negative effects of *H. pylori* on *M. bovis* control and boosts *M. bovis* clearance (Figures 5H and 5I), prevents the redirection of Treg cells to the liver and favors the generation of Foxp3$^-$ effectors (Figures S6C–S6E). The combined results are consistent with the notion that *M. bovis* recruits and redirects Treg cells to the liver, where they suppress anti-mycobacterial T cell responses and impair BCG clearance; prior immunization reverses both the redirection of Treg cells and the detrimental effects of *H. pylori* on *M. bovis* immune control. Conversely, the relative under-representation of Treg cells in the gastric mucosa of co-infected mice leads to derepressed gastric T cell responses and the associated improved immune control of *H. pylori* on the one hand and aggravated immunopathology on the other.

Blockade of Treg cell recruitment to the liver reverses the detrimental effects of *H. pylori* on *M. bovis* immune control

We have shown in earlier work that gastric RORγt$^+$ Tbet$^+$ Nrp$^-$ Treg cells are induced to express the surface receptor CXCR3

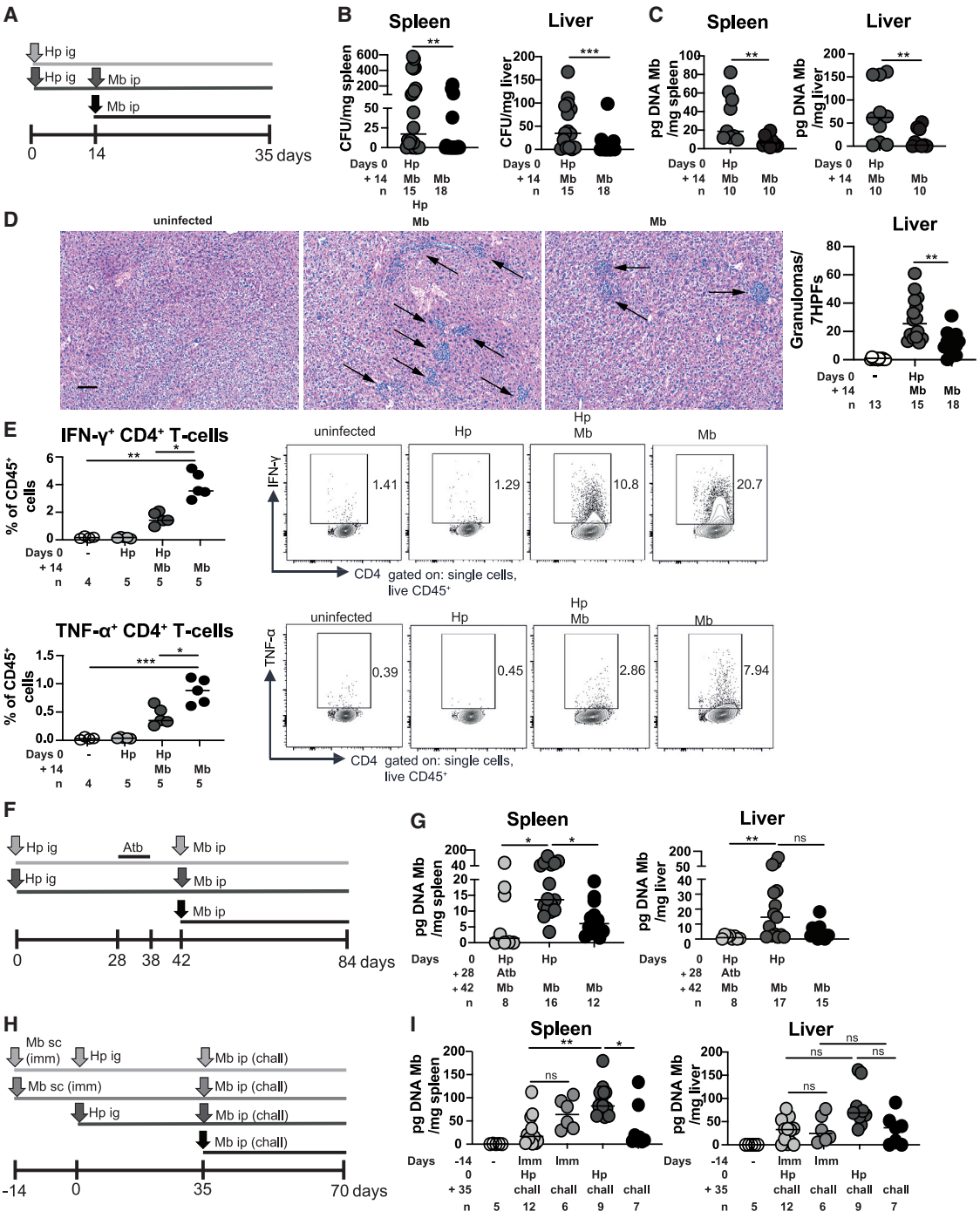

Figure 5. Active *H. pylori* infection compromises immune control of *M. bovis* at distant sites

(A) Schematic of the sequence of i.p. *M. bovis* and i.g. *H. pylori* infection of the groups shown in (B)–(E).

(B) *M. bovis* colonization of the spleen and liver, represented as CFUs per mg of tissue, of mice that were infected as shown in (A).

(C) *M. bovis* colonization of the spleen and liver as detected and quantified (in pg DNA/mg of tissue) by qPCR using genomic DNA as template.

(D) Liver granulomas as quantified in a total of seven high-powered fields of H&E-stained livers of mice infected as shown in (A). Representative images are shown alongside summary plots of all mice. The scale bar indicates 100 μm. Arrows point to granulomas.

(E) Frequencies of IFN-γ^+ or TNF-α^+ CD4$^+$ T cells among all hepatic CD45$^+$ leukocytes as determined by intracellular cytokine staining upon PPD-specific re-stimulation of mice that were infected as shown in (A) or remained uninfected. Representative FACS plots are shown alongside summary plots of all mice. Data in (B) and (D) are pooled from three studies and in (C) from two studies; data in (E) are from one study.

(F) Schematic of the sequence of i.p. *M. bovis* and i.g. *H. pylori* infection and of antibiotic eradication therapy of the groups shown in (G).

(legend continued on next page)

during the priming phase in lymph nodes; CXCR3 expression allows these cells to follow a chemokine gradient, formed by CXCL9 and CXCL10, to infected and inflamed tissues (Arnold et al., 2019). Indeed, not only gastric but also liver-resident Treg cells expressing RORγt and Tbet are positive for CXCR3, a known target of the transcription factor Tbet (Littringer et al., 2018); this is not the case for RORγt$^-$ Tbet$^-$ Treg cells (Figure 7A). Interestingly, *M. bovis*-infected livers express 10- to 100-fold higher levels, as assessed by qRT-PCR, of the Treg cell chemoattractants CXCL9 and CXCL10 than the *H. pylori* (or *M. bovis*-)-infected gastric mucosa (Figure 7B). Based on these observations, we asked whether antibody-mediated blockade of the CXCL9/10/CXCR3 signaling axis would affect gastric and liver Treg cell populations and colonization levels of both bacteria (Figure 7C). Whereas gastric Treg cell populations and *H. pylori* colonization levels were not measurably affected by CXCR3 blockade in co-infected mice (Figures S7A and S7B), we observed a strong reduction in the frequencies and absolute numbers of hepatic Nrp-1$^-$ Treg cells and RORγt$^+$ Nrp-1$^-$ Treg cells as a result of CXCR3 blockade (Figures 7D and 7E). *M. bovis* clearance, which was impaired by the presence of *H. pylori* in the stomach of co-infected mice, was restored by CXCR3 blockade in both the liver and the spleen (Figures 7F and 7G); the restored *M. bovis* clearance was reflected in reduced numbers of liver granulomas (Figure 7H). In summary, these results are consistent with the interpretation that the presence of *H. pylori* in the gastric mucosa results in the *de novo* priming of Treg cells, which—rather than migrate to the site of *H. pylori* infection—are recruited to the *M. bovis*-infected liver in a CXCR3-dependent manner; their excessive presence in the liver likely compromises clearance of *M. bovis*.

DISCUSSION

Our work on an experimental co-infection model of *H. pylori* and *M. bovis*, which was designed to mimic the projected co-occurrence of *H. pylori* and Mtb in at least one-eighth and possibly up to one-fifth of the human population, yielded several unexpected insights into the mutual interaction of the two pathogens. The effects of each bacterium on the respective other species tended to be more pronounced if the first pathogen had been given time to establish itself and if some level of chronicity had been reached before exposure of the host to the second pathogen. Both pathogens are known to infect children, adolescents, and young adults. Infection with *H. pylori* peaks in the earliest years of life; in fact, in endemic regions, the majority of children are believed to have contracted the infection from family members before their second birthday (Weyermann et al., 2009). The risk of infection with Mtb is highest during adolescence and young adulthood (Morabia, 2014). Sequential infection with both pathogens therefore is conceivable, and the consecutive exposure to *H. pylori* first and Mtb second is particularly plausible in many geographical areas of the world in which both *H. pylori* and Mtb are highly prevalent.

We first examined in detail the consequences of *M. bovis* presence on *H. pylori* colonization, on anti-*H. pylori* immune responses, and on infection-associated gastric immunopathology. We used two alternative routes of *M. bovis* administration, i.e., either i.p. with the objective of targeting the liver and spleen or i.n. targeting the lung. *M. bovis* administered via either of the two routes strongly enhanced immune control of *H. pylori* and resulted in at least a 5-fold reduction in *H. pylori* colonization levels; this effect was stable for up to 3 months post-infection. The improved clearance of *H. pylori* was accompanied by strongly enhanced Th1 and humoral immune responses and resulted in more severe and more widespread immunopathology. Gastric inflammation, atrophy, and metaplasia were all more pronounced in co-infected mice relative to mice infected with *H. pylori* only. Our own and others' prior data all point to these lesions as being of immunopathological origin; T cells, and in particular, Th1-polarized, cytokine-expressing CD4$^+$ T cells as well as CD8$^+$ T cells, drive the development of such preneoplastic lesions (Arnold et al., 2011a; Gray et al., 2013; Sayi et al., 2009; Sun et al., 2017; Wustner et al., 2017). In fact, the transgenic expression of the Th1 signature cytokine IFN-γ in the gastric mucosa is sufficient to induce metaplasia and dysplasia, even in the absence of *H. pylori* (Syu et al., 2012). The combined data from both short- and long-term co-infection settings support the conclusion that the presence of *M. bovis* boosts anti-*H. pylori* immunity, which results in more severe Th1-driven immunopathology. These findings are reminiscent of co-infection of the close *H. pylori* relative *Helicobacter felis* with the protozoan parasite *Toxoplasma gondii*, which, just like *M. bovis*, enhances gastric Th1 cytokine responses and drives more severe gastric mucosal inflammation, parietal cell loss, atrophy, and metaplasia (Stoicov et al., 2004); a human correlate exists for this observation in Colombians infected with *T. gondii*, who tend to have higher titers of (Th1-dependent) immunoglobulin G2 (IgG2) antibodies to *H. pylori* than their *T. gondii*-negative counterparts (Ek et al., 2012).

Quite the opposite effect is seen on *M. bovis* colonization and anti-*M. bovis* immune responses if *H. pylori* is present. *M. bovis* immune control is impaired by the presence of *H. pylori* in the stomach, and this observation is consistent in all tissues in which (live) *M. bovis* can be detected by either plating or PCR-based techniques. Antibiotic eradication therapy that successfully eliminates *H. pylori* and prior subcutaneous immunization with live *M. bovis* both restore immune control of a subsequent *M. bovis* challenge infection, which together indicate that an ongoing, active (not just past) infection with *H. pylori* is required

(G) *M. bovis* colonization of the spleen and liver as detected and quantified (in pg DNA/mg of tissue) by qPCR using genomic DNA as template. Data in (G) are pooled from two independent studies.
(H) Schematic of the sequence of i.p. *M. bovis* and i.g. *H. pylori* infection and of prior subcutaneous (s.c.) immunization with live *M. bovis* of the groups shown in (I).
(I) *M. bovis* colonization of the spleen and liver as detected and quantified (in pg DNA/mg of tissue) by qPCR using genomic DNA as template. Data in (I) are pooled from two independent studies.
Statistical comparisons were done by Mann-Whitney (two groups) or Kruskal-Wallis test with Dunn's post-hoc test (more than two groups). Only relevant comparisons are shown. *$p < 0.05$, **$p < 0.01$, and ***$p < 0.001$. n indicates the number of mice per group. See also Figure S5.

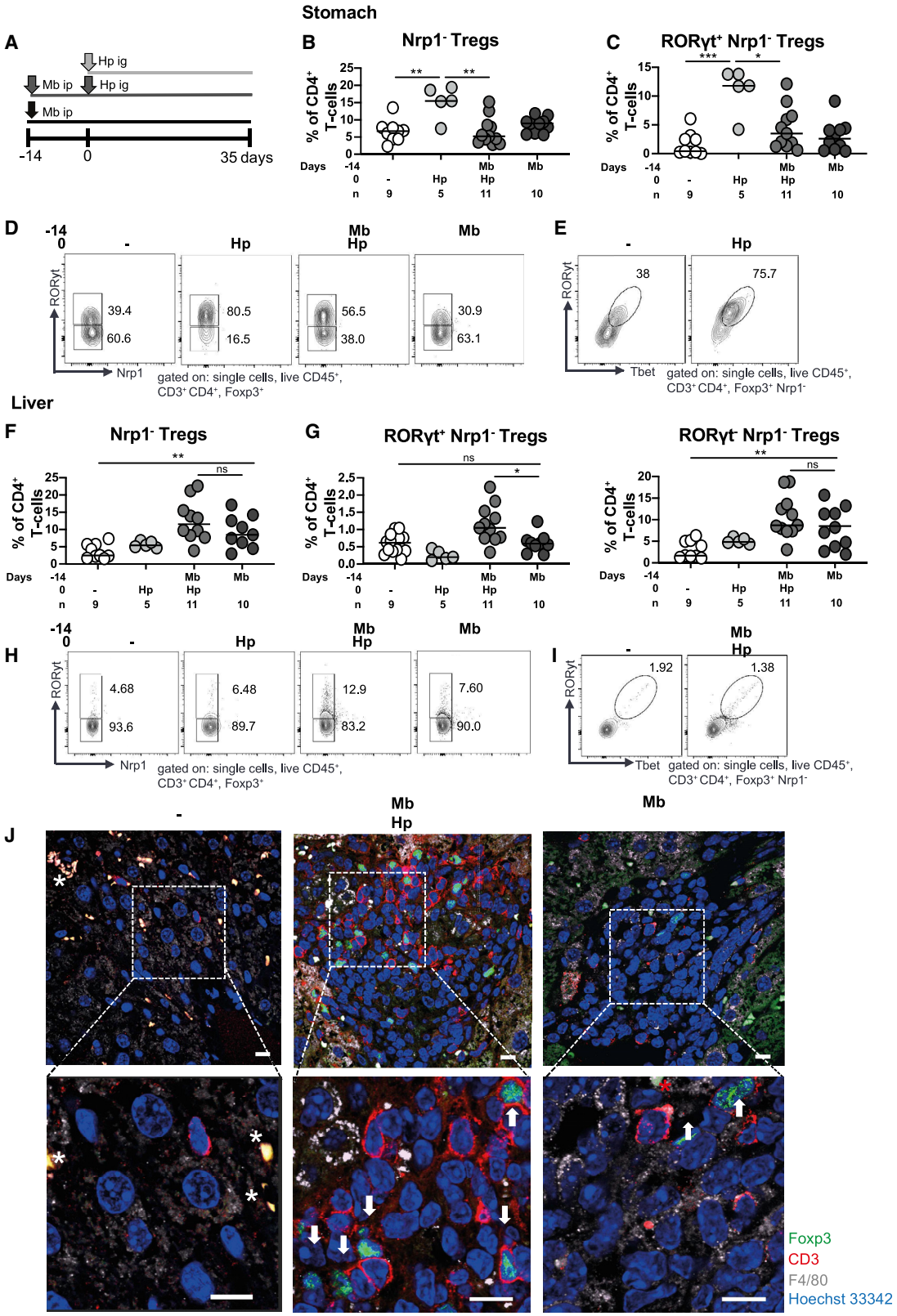

(legend on next page)

for such immunomodulation to occur. Prior immunization skews liver anti-mycobacterial T cell responses toward effector T cells at the expense of Treg cells and overcomes the immunomodulatory effects of a co-occurring *H. pylori* infection.

Two alternative mechanistic scenarios can potentially explain the mutual interaction of both pathogens and both were examined in this study. We first hypothesized that each bacterium might unexpectedly inhabit the other's preferred tissue of residence and directly affect immune responses and tissue homeostasis locally. Whereas *H. pylori* could not be detected in the liver or spleen (data not shown) and indeed is not known to reside in tissues other than the gastric mucosa, we collected substantial evidence for the presence of *M. bovis* in the stomach and other tissues of the gastrointestinal tract and were also able to detect Mtb DNA in whole-exome and whole-genome sequencing data from human stomach tissue—both normal and cancerous. Indeed, *M. bovis* (mono-) residence in the stomach triggered a strong and reproducible local T cell response that was dominated by a characteristic population of multifunctional $CD4^+$ T cells co-expressing TNF-α, IL-10, and IFN-γ; such cells were absent in the uninfected and in the *H. pylori* single-infected gastric mucosa. *M. bovis* infection alone, despite its impact on the gastric T cell compartment, failed to cause gastric immunopathology in the murine model, even after 3 months of exposure. In human gastric cancer, the prevalence of Mtb DNA is higher than the Mtb positivity rate in the general population, as assessed via tuberculin skin test or other immunological parameters (Miramontes et al., 2015), and approximately half of Mtb-positive cancer cases additionally exhibit evidence of *H. pylori* presence. There was no bias in Mtb positivity toward a specific genetic subtype of gastric cancer, and the transcriptomes and tumor microenvironment of Mtb-positive and -negative cases did not appear to differ much. However, we observed a genetic signature of 79 genes that were significantly more commonly mutated—across all four genetic subtypes of gastric cancer—in the Mtb-positive cases, which potentially points to a role of the Mtb status of the patient in shaping the genetic landscape of the corresponding tumor.

An alternative hypothesis that can plausibly explain the mutual interaction of mycobacteria and *H. pylori* takes into account long-distance effects of infected tissues on other sites of the body. We and others have previously shown that both effector and regulatory $CD4^+$ T cells are recruited to infected and inflamed tissues along a gradient of the chemokines CXCL9 and CXCL10, which are produced mainly be myeloid cells and specifically attract $CXCR3^+$ $CD4^+$ T cells (Arnold et al., 2019; Littringer et al., 2018). CXCR3 is expressed by both Th1-polarized effector T cells and Treg cells that have been generated in settings of type 1 immunity (Littringer et al., 2018), not only in the gastrointestinal (GI) tract and in tumor tissues as shown previously (Arnold et al., 2019) but also in the liver as shown here. CXCR3 expression is controlled by the transcription factor Tbet (Littringer et al., 2018). Interestingly, we observed a redirection of $CXCR3^+$ Treg cells to the liver in settings of *M. bovis* and *H. pylori* co-infection; the net result of this redirection is a relative under-representation of *de novo* induced $ROR\gamma t^+$ $Tbet^+$ $Nrp\text{-}1^-$ Treg cells in the *H. pylori*-infected stomach and their over-representation in the *M. bovis*-infected liver. This redirection appeared to be the consequence of the much steeper CXCL9/CXCL10 gradient produced by the infected liver than the infected stomach, as CXCR3 neutralization blocked Treg cell recruitment to the liver. Indeed, blocking Treg cell recruitment to the liver restored *M. bovis* clearance and reversed the negative effects of *H. pylori* on *M. bovis* clearance. As Treg cell recruitment to the stomach is also compromised by CXCR3 neutralization (Arnold et al., 2019), no effects were expected or observed on *H. pylori* control in this setting. The mechanisms through which $CXCR3^+$ Treg cells suppress *M. bovis* control are subject to further studies and likely involve regulatory effects on various CD4 and CD8 and possibly innate immune lymphocyte populations.

Very little evidence exists from human observational studies or other experimental studies that would address the mutual interactions of mycobacteria and *Helicobacter* species. The studies available so far have focused exclusively on the effects of *Helicobacter* species on Mtb immunity and lung pathology, not the other way around. An observational study conducted on household contacts of tuberculosis (TB) patients revealed that contacts who went on to develop TB within a 2-year follow-up period were significantly less likely to be *H. pylori* infected than contacts who did not develop TB (Perry et al., 2010). In the same study, cynomolgus macaques with natural *H. pylori* infection were found to be less likely to progress to TB 6–8 months after an experimental Mtb challenge, together suggesting that *H. pylori* confers protection against TB (Perry et al., 2010). These results are in contrast to two independent studies using experimental Mtb infection in mice in which natural colonization with *Helicobacter hepaticus*, a constituent of the normal murine cecal, colonic, and biliary tract microbiota, aggravated Mtb-induced lung

Figure 6. *M. bovis* infection redirects *de novo* generated Treg cells to the liver

(A) Schematic of the sequence of i.p. *M. bovis* and i.g. *H. pylori* infection of the groups shown in (B)–(J).

(B–D) Frequencies of gastric neuropilin-1 (Nrp1)-negative, $Foxp3^+$ Treg cells among all $CD4^+$ T cells (B) and of gastric $ROR\gamma t^+$ $Nrp1^-$ Treg cells among all $CD4^+$ T cells (C) of mice infected as shown in (A). Representative contour plots are shown for all groups in (D).

(E) Gastric $ROR\gamma t^+$ $Nrp1^-$ Treg cells express Tbet during *H. pylori* infection. A representative contour plot is shown.

(F–H) Frequencies of hepatic $Nrp1^-$ $Foxp3^+$ Treg cells among all $CD4^+$ T cells (F) and of hepatic $ROR\gamma t^+$ $Nrp1^-$ Treg cells and of $ROR\gamma t^-$ $Nrp1^-$ Treg cells (G) of the groups shown in (B) and (C). Representative contour plots are shown for all groups in (H).

(I) Hepatic $ROR\gamma t^+$ $Nrp1^-$ Treg cells express Tbet. A representative contour plot is shown.

(J) Representative immunofluorescence microscopy images of hepatic FFPE sections of an uninfected (–) mouse, an *M. bovis*-infected mouse, and a mouse that was first infected with *M. bovis* and subsequently with *H. pylori*, stained with antibodies specific for Foxp3 (green), CD3 (red), and F4/80 (gray) as well as with Hoechst 33,342. The magnification of the selected areas is depicted below each image. The white arrows point to $Foxp3^+$ $CD3^+$ Treg cells. The white asterisks indicate unspecific autofluorescence of red blood cells. Scale bars indicate 10 μm.

Data in (B), (C), (F), and (G) are pooled from two independent experiments. Statistical comparisons were done by Kruskal-Wallis test with Dunn's post-hoc test. Only relevant comparisons are shown. *$p < 0.05$, **$p < 0.01$, and ***$p < 0.001$. n indicates the number of mice per group. See also Figure S6.

CellPress
OPEN ACCESS

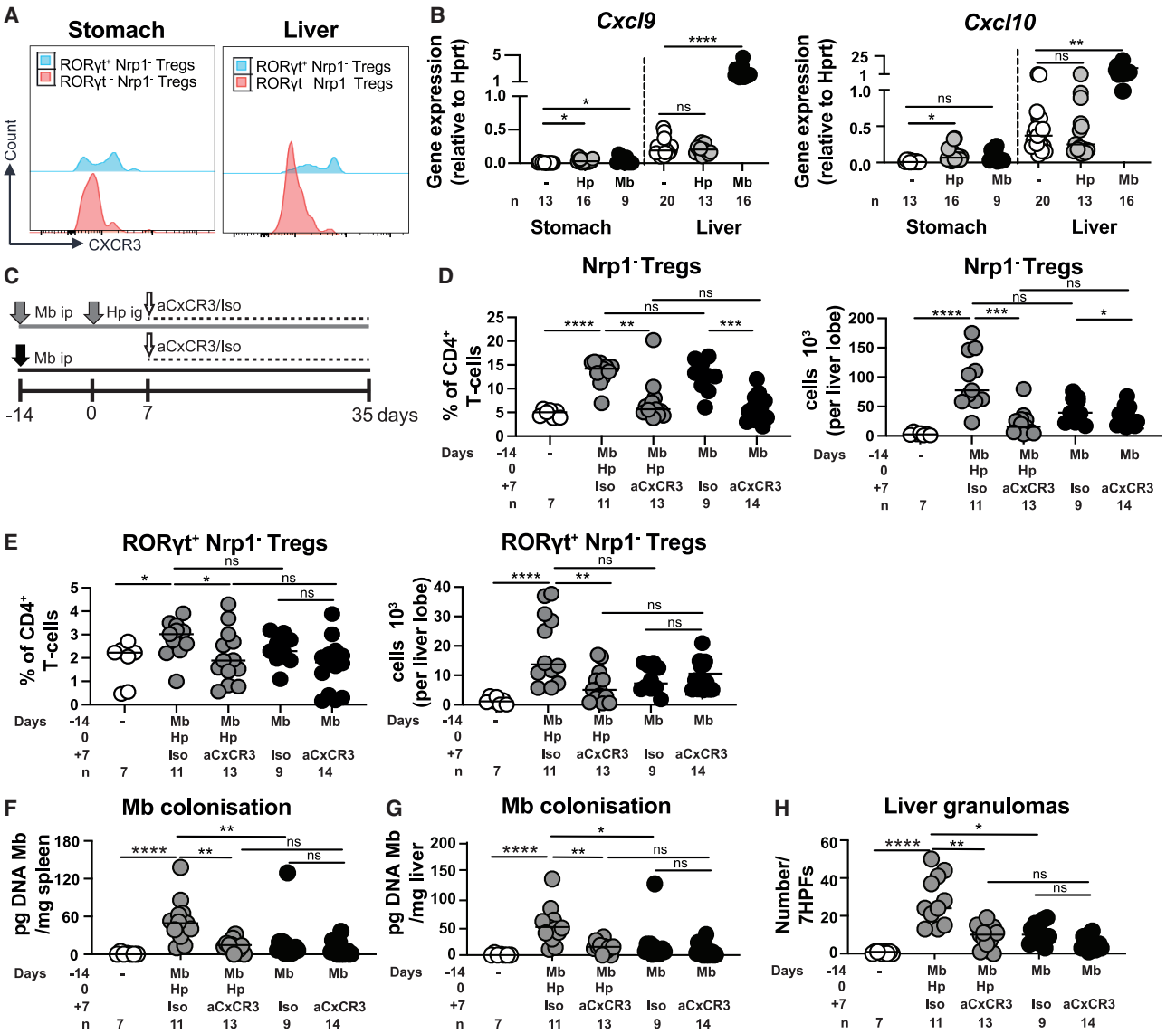

Figure 7. Neutralization of CXCR3 reverses the detrimental effects of *H. pylori* on *M. bovis* control in the liver

(A) CXCR3 expression of gastric and hepatic RORγt$^+$ Nrp1$^-$ Treg cells and of RORγt$^-$ Nrp1$^-$ Treg cells; representative histograms are shown of a co-infected mouse.

(B) Transcript levels of the indicated cytokines as assessed by qRT-PCR of gastric and liver tissue of mice infected for 5 weeks with either *H. pylori* or *M. bovis*. Gene expression is normalized to the housekeeping gene *Hprt*.

(C) Schematic of the sequence of i.p. *M. bovis* and i.g. *H. pylori* infection and of CXCR3 neutralizing antibody or control isotype treatment of the groups shown in (D)–(H).

(D and E) Frequencies among all CD4$^+$ T cells and absolute numbers of hepatic Nrp1$^-$ Foxp3$^+$ Treg cells (D) and of hepatic RORγt$^+$ Nrp1$^-$ Treg cells (E) of the groups infected and treated as shown in (C).

(F and G) *M. bovis* colonization of the spleen and liver as detected and quantified (in pg DNA/mg of tissue) by qPCR using genomic DNA as template of the groups infected and treated as shown in (C).

(H) Liver granulomas as quantified in a total of seven high-powered fields of H&E-stained livers of mice infected and treated as shown in (C). Data in (F)–(H) are pooled from three independent studies; data in (D) and (E) are from two independent studies. Statistical comparisons were done by Kruskal-Wallis test followed by Dunn's post-hoc test. Only relevant comparisons are shown. *$p < 0.05$, **$p < 0.01$, ***$p < 0.001$, and ****$p < 0.0001$. n indicates the number of mice per group. See also Figure S7.

pathology (Arnold et al., 2015; Majlessi et al., 2017). Given the broad relevance of the problem, the enormous global disease burden associated with both pathogens, and the striking findings reported in the few available studies, more work is clearly needed on experimental models and human populations alike.

Limitations of the study

Our study has several important limitations. First, for practical reasons, we use *M. bovis* instead of the more relevant Mtb in our work. Mtb is a biosafety level 3 pathogen, and few facilities exist worldwide in which research on Mtb can be

performed; we do not have access to such a facility. While *M. bovis* recapitulates several important features of Mtb infection, such as the latter's persistence, ability to induce granuloma formation, and strong Th1-polarizing capacity, it fails to phenocopy Mtb-induced pulmonary and extrapulmonary diseases. A second limitation is our predominant (but not exclusive) reliance on the i.p. infection route, which results in systemic colonization of various organs, including the spleen and liver, but not the lung (i.e., the main site of Mtb colonization). The few studies we are showing here using i.n. infection (leading to pulmonary colonization of *M. bovis*) confirmed a strong effect of lung-resident *M. bovis* on *H. pylori* colonization and *H. pylori*-specific Th1 responses in the gastric mucosa; however, the reverse experiment, designed to elucidate how *H. pylori* affects pulmonary colonization, lung immune responses, and lung immunopathology induced by *M. bovis*, was not done. Finally, our work on Treg cells and T cells in general is hampered by the lack of *H. pylori*-specific T cell receptor (TCR)-transgenic mouse lines. Such a line exists for the closely related *H. hepaticus* and has led to exciting new insights into the biology of bacteria-specific Treg cells and the role of the transcription factor c-MAF in Treg cell function and GI immune homeostasis (Xu et al., 2018). Comparable transgenic mouse lines do not exist for *H. pylori* but would have been extremely useful in the current study for the purpose of tracking redirected *H. pylori*-specific Treg cells to extragastric sites. In summary, more effort needs to be invested into the development of new tools, relevant infection models, and routes of infection in order to address some of the limitations listed above.

STAR METHODS

Detailed methods are provided in the online version of this paper and include the following:

- KEY RESOURCES TABLE
- RESOURCE AVAILABILITY
  - Lead contact
  - Materials availability
  - Data and code availability
- EXPERIMENTAL MODEL AND SUBJECT DETAILS
  - Mouse experimentation
- METHOD DETAILS
  - Assessment of gastric histopathology
  - Leukocyte isolation
  - Flow cytometry, T-cell re-stimulation and cell sorting
  - Multiplex serology
  - Quantitative PCR
  - Immunofluorescence and confocal microscopy
  - TCGA data analysis and annotation of *H. pylori* and Mtb status
- QUANTIFICATION AND STATISTICAL ANALYSIS

SUPPLEMENTAL INFORMATION

Supplemental information can be found online at https://doi.org/10.1016/j.celrep.2022.110359.

ACKNOWLEDGMENTS

This work was supported by the Swiss National Science Foundation (BSCGIO_157841/1 and 310030_192490 to A.M. and 310030_184816 to H.-U.S.). H.-U.S. acknowledges financial support by the Russian Government Program "Recruitment of the Leading Scientists into the Russian Institutions of Higher Education" (075-15-2021-600). The sponsors had no role in the study design, data analysis, or any other part of the research and manuscript submission. The authors wish to thank all members of the Müller lab for helpful discussions.

AUTHOR CONTRIBUTIONS

M.A.-B., A.F., M.P., S.W., and J.H. conducted all experiments; S.Y. and H.-U.S. stained formalin-fixed, paraffin-embedded (FFPE) sections. A.B.D., X.S., M.P.L., and P.F.C. performed bioinformatic analyses of TCGA data. R.J. and T.W. contributed multiplex *H. pylori* ELISA data. A.M. supervised the study.

DECLARATION OF INTERESTS

The authors declare no competing interests.

Received: July 22, 2021
Revised: November 12, 2021
Accepted: January 19, 2022
Published: February 8, 2022

REFERENCES

Arnold, I.C., Hutchings, C., Kondova, I., Hey, A., Powrie, F., Beverley, P., and Tchilian, E. (2015). Helicobacter hepaticus infection in BALB/c mice abolishes subunit-vaccine-induced protection against M. tuberculosis. Vaccine *33*, 1808–1814.

Arnold, I.C., Lee, J.Y., Amieva, M.R., Roers, A., Flavell, R.A., Sparwasser, T., and Muller, A. (2011a). Tolerance rather than immunity protects from Helicobacter pylori-induced gastric preneoplasia. Gastroenterology *140*, 199–209.

Arnold, I.C., Lee, J.Y., Amieva, M.R., Roers, A., Flavell, R.A., Sparwasser, T., and Müller, A. (2011b). Tolerance rather than immunity protects from Helicobacter pylori-induced gastric preneoplasia. Gastroenterology *140*, 199–209.

Arnold, I.C., Zhang, X., Artola-Boran, M., Fallegger, A., Sander, P., Johansen, P., and Muller, A. (2019). BATF3-dependent dendritic cells drive both effector and regulatory T-cell responses in bacterially infected tissues. PLoS Pathog. *15*, e1007866.

Bae, J.M., and Kim, E.H. (2016). Epstein-barr virus and gastric cancer risk: a meta-analysis with meta-regression of case-control studies. J. Prev. Med. Public Health *49*, 97–107.

Bass, A.J., Thorsson, V., Shmulevich, I., Reynolds, S.M., Miller, M., Bernard, B., Hinoue, T., Laird, P.W., Curtis, C., Shen, H., et al. (2014). Comprehensive molecular characterization of gastric adenocarcinoma. Nature *513*, 202–209.

Chen, B., Khodadoust, M.S., Liu, C.L., Newman, A.M., and Alizadeh, A.A. (2018). Profiling tumor infiltrating immune cells with CIBERSORT. Methods Mol. Biol. *1711*, 243–259.

Chen, X.Y., van der Hulst, R.W., Bruno, M.J., van der Ende, A., Xiao, S.D., Tytgat, G.N., and Ten Kate, F.J. (1999). Interobserver variation in the histopathological scoring of Helicobacter pylori related gastritis. J. Clin. Pathol. *52*, 612–615.

Colaprico, A., Silva, T.C., Olsen, C., Garofano, L., Cava, C., Garolini, D., Sabedot, T.S., Malta, T.M., Pagnotta, S.M., Castiglioni, I., et al. (2016). TCGAbiolinks: an R/Bioconductor package for integrative analysis of TCGA data. Nucleic Acids Res. *44*, e71.

Crabtree, J.E., and Wessler, S. (2018). Special issue "H-pylori virulence factors in the induction of gastric cancer". Toxins *10*, 176.

Dohlman, A.B., Arguijo Mendoza, D., Ding, S., Gao, M., Dressman, H., Iliev, I.D., Lipkin, S.M., and Shen, X. (2021). The cancer microbiome atlas: a pan-

cancer comparative analysis to distinguish tissue-resident microbiota from contaminants. Cell Host Microbe *29*, 281–298.e5.

Ek, C., Whary, M.T., Ihrig, M., Bravo, L.E., Correa, P., and Fox, J.G. (2012). Serologic evidence that ascaris and toxoplasma infections impact inflammatory responses to Helicobacter pylori in Colombians. Helicobacter *17*, 107–115.

Erb, K.J., Holloway, J.W., Sobeck, A., Moll, H., and Le Gros, G. (1998). Infection of mice with Mycobacterium bovis-Bacillus Calmette-Guerin (BCG) suppresses allergen-induced airway eosinophilia. J. Exp. Med. *187*, 561–569.

Gray, B.M., Fontaine, C.A., Poe, S.A., and Eaton, K.A. (2013). Complex T cell interactions contribute to Helicobacter pylori gastritis in mice. Infect. Immun. *81*, 740–752.

Gu, Z., Eils, R., and Schlesner, M. (2016). Complex heatmaps reveal patterns and correlations in multidimensional genomic data. Bioinformatics *32*, 2847–2849.

Hooi, J.K.Y., Lai, W.Y., Ng, W.K., Suen, M.M.Y., Underwood, F.E., Tanyingoh, D., Malfertheiner, P., Graham, D.Y., Wong, V.W.S., Wu, J.C.Y., et al. (2017). Global prevalence of Helicobacter pylori infection: systematic review and meta-analysis. Gastroenterology *153*, 420–429.

Horsburgh, C.R., Jr., and Rubin, E.J. (2011). Clinical practice. Latent tuberculosis infection in the United States. N. Engl. J. Med. *364*, 1441–1448.

Houben, R.M., and Dodd, P.J. (2016). The global burden of latent tuberculosis infection: a Re-estimation using mathematical modelling. PLoS Med. *13*, e1002152.

Kostic, A.D., Ojesina, A.I., Pedamallu, C.S., Jung, J., Verhaak, R.G., Getz, G., and Meyerson, M. (2011). PathSeq: software to identify or discover microbes by deep sequencing of human tissue. Nat. Biotechnol. *29*, 393–396.

Law, C.W., Chen, Y., Shi, W., and Smyth, G.K. (2014). voom: precision weights unlock linear model analysis tools for RNA-seq read counts. Genome Biol. *15*, R29.

Lee, A., O'Rourke, J., De Ungria, M.C., Robertson, B., Daskalopoulos, G., and Dixon, M.F. (1997). A standardized mouse model of Helicobacter pylori infection: introducing the Sydney strain. Gastroenterology *112*, 1386–1397.

Lesellier, S., Boschiroli, M.L., Barrat, J., Wanke, C., Salguero, F.J., Garcia-Jimenez, W.L., Nunez, A., Godinho, A., Spiropoulos, J., Palmer, S., et al. (2019). Detection of live M. bovis BCG in tissues and IFN-gamma responses in European badgers (Meles meles) vaccinated by oropharyngeal instillation or directly in the ileum. BMC Vet. Res. *15*, 445.

Littringer, K., Moresi, C., Rakebrandt, N., Zhou, X., Schorer, M., Dolowschiak, T., Kirchner, F., Rost, F., Keller, C.W., McHugh, D., et al. (2018). Common features of regulatory T cell specialization during Th1 responses. Front. Immunol. *9*, 1344.

Majlessi, L., Sayes, F., Bureau, J.F., Pawlik, A., Michel, V., Jouvion, G., Huerre, M., Severgnini, M., Consolandi, C., Peano, C., et al. (2017). Colonization with Helicobacter is concomitant with modified gut microbiota and drastic failure of the immune control of Mycobacterium tuberculosis. Mucosal Immunol. *10*, 1178–1189.

Michel, A., Waterboer, T., Kist, M., and Pawlita, M. (2009). Helicobacter pylori multiplex serology. Helicobacter *14*, 525–535.

Miramontes, R., Hill, A.N., Yelk Woodruff, R.S., Lambert, L.A., Navin, T.R., Castro, K.G., and LoBue, P.A. (2015). Tuberculosis infection in the United States: prevalence estimates from the National Health and Nutrition Examination Survey, 2011-2012. PLoS One *10*, e0140881.

Morabia, A. (2014). Snippets from the past: cohort analysis of disease rates-another piece in a seemingly still incomplete puzzle. Am. J. Epidemiol. *180*, 189–196.

Newman, A.M., Liu, C.L., Green, M.R., Gentles, A.J., Feng, W., Xu, Y., Hoang, C.D., Diehn, M., and Alizadeh, A.A. (2015). Robust enumeration of cell subsets from tissue expression profiles. Nat. Methods *12*, 453–457.

Parsonnet, J., Friedman, G.D., Vandersteen, D.P., Chang, Y., Vogelman, J.H., Orentreich, N., and Sibley, R.K. (1991). Helicobacter pylori infection and the risk of gastric carcinoma. N. Engl. J. Med. *325*, 1127–1131.

Peek, R.M., Jr., and Blaser, M.J. (2002). Helicobacter pylori and gastrointestinal tract adenocarcinomas. Nat. Rev. Cancer *2*, 28–37.

Perry, S., de Jong, B.C., Solnick, J.V., de la Luz Sanchez, M., Yang, S., Lin, P.L., Hansen, L.M., Talat, N., Hill, P.C., Hussain, R., et al. (2010). Infection with Helicobacter pylori is associated with protection against tuberculosis. PLoS one *5*, e8804.

Rawla, P., and Barsouk, A. (2019). Epidemiology of gastric cancer: global trends, risk factors and prevention. Prz. Gastroenterol. *14*, 26–38.

Savage, P.A., Klawon, D.E.J., and Miller, C.H. (2020). Regulatory T cell development. Annu. Rev. Immunol. *38*, 421–453.

Saxena, R.K., Weissman, D., Simpson, J., and Lewis, D.M. (2002). Murine model of BCG lung infection: dynamics of lymphocyte subpopulations in lung interstitium and tracheal lymph nodes. J. Biosci. *27*, 143–153.

Sayi, A., Kohler, E., Hitzler, I., Arnold, I., Schwendener, R., Rehrauer, H., and Muller, A. (2009). The CD4+ T cell-mediated IFN-gamma response to Helicobacter infection is essential for clearance and determines gastric cancer risk. J. Immunol. *182*, 7085–7101.

Sayi, A., Kohler, E., Toller, I.M., Flavell, R.A., Muller, W., Roers, A., and Müller, A. (2011). TLR-2-activated B cells suppress Helicobacter-induced preneoplastic gastric immunopathology by inducing T regulatory-1 cells. J. Immunol. *186*, 878–890.

Stoicov, C., Whary, M., Rogers, A.B., Lee, F.S., Klucevsek, K., Li, H., Cai, X., Saffari, R., Ge, Z., Khan, I.A., et al. (2004). Coinfection modulates inflammatory responses and clinical outcome of Helicobacter felis and Toxoplasma gondii infections. J. Immunol. *173*, 3329–3336.

Sun, X., Zhang, M., El-Zaatari, M., Huffnagle, G.B., and Kao, J.Y. (2017). CCR2 mediates Helicobacter pylori-induced immune tolerance and contributes to mucosal homeostasis. Helicobacter *22*, e12366.

Syu, L.J., El-Zaatari, M., Eaton, K.A., Liu, Z., Tetarbe, M., Keeley, T.M., Pero, J., Ferris, J., Wilbert, D., Kaatz, A., et al. (2012). Transgenic expression of interferon-gamma in mouse stomach leads to inflammation, metaplasia, and dysplasia. Am. J. Pathol. *181*, 2114–2125.

Uemura, N., Okamoto, S., Yamamoto, S., Matsumura, N., Yamaguchi, S., Yamakido, M., Taniyama, K., Sasaki, N., and Schlemper, R.J. (2001). Helicobacter pylori infection and the development of gastric cancer. N. Engl. J. Med. *345*, 784–789.

Waterboer, T., Sehr, P., Michael, K.M., Franceschi, S., Nieland, J.D., Joos, T.O., Templin, M.F., and Pawlita, M. (2005). Multiplex human papillomavirus serology based on in situ-purified glutathione s-transferase fusion proteins. Clin. Chem. *51*, 1845–1853.

Weyermann, M., Rothenbacher, D., and Brenner, H. (2009). Acquisition of Helicobacter pylori infection in early childhood: independent contributions of infected mothers, fathers, and siblings. Am. J. Gastroenterol. *104*, 182–189.

Wustner, S., Anderl, F., Wanisch, A., Sachs, C., Steiger, K., Nerlich, A., Vieth, M., Mejias-Luque, R., and Gerhard, M. (2017). Helicobacter pylori gamma-glutamyl transferase contributes to colonization and differential recruitment of T cells during persistence. Sci. Rep. *7*, 13636.

Xu, M., Pokrovskii, M., Ding, Y., Yi, R., Au, C., Harrison, O.J., Galan, C., Belkaid, Y., Bonneau, R., and Littman, D.R. (2018). c-MAF-dependent regulatory T cells mediate immunological tolerance to a gut pathobiont. Nature *554*, 373–377.

Yusefi, A.R., Bagheri Lankarani, K., Bastani, P., Radinmanesh, M., and Kavosi, Z. (2018). Risk factors for gastric cancer: a systematic review. Asian Pac. J. Cancer Prev. *19*, 591–603.

Zamani, M., Ebrahimtabar, F., Zamani, V., Miller, W.H., Alizadeh-Navaei, R., Shokri-Shirvani, J., and Derakhshan, M.H. (2018). Systematic review with meta-analysis: the worldwide prevalence of Helicobacter pylori infection. Aliment. Pharmacol. Ther. *47*, 868–876.

Zhang, X., Artola-Boran, M., Fallegger, A., Arnold, I.C., Weber, A., Reuter, S., Taube, C., and Muller, A. (2020). IRF4 expression is required for the immunoregulatory activity of conventional type 2 dendritic cells in settings of chronic bacterial infection and cancer. J. Immunol. *205*, 1933–1943.

STAR METHODS

KEY RESOURCES TABLE

REAGENT or RESOURCE	SOURCE	IDENTIFIER
Antibodies		
anti-mouse CD45	BioLegend	Clone 30-F11; RRID: AB_657749
anti-mouse CD4	BioLegend	Clone RM4-5; RRID: AB_893325
anti-mouse CD8	BioLegend	Clone 53-6.7; RRID: AB_2738084
anti-mouse TCRβ	BioLegend	Clone H57-597; RRID: AB_10644003
anti-mouse Neuropilin-1	BioLegend	Clone 3E12; RRID: AB_2562033
IgG isotype	BioLegend	RRID: AB_1107773
FCblock	Affymetrix	anti-CD16/CD32; RRID: AB_467133
anti-mouse IL-17A	Invitrogen	Clone TC11-18H10.1; RRID: AB_2125010
anti-mouse IFN-γ	Invitrogen	Clone XMG1.2; RRID: AB_1595591
anti-mouse TNF-α	Invitrogen	Clone MP6-XT22; RRID: AB_2721314
anti-mouse FoxP3	Invitrogen	Clone FJK-16s; RRID: AB_2865134
anti-mouse RORγt	Invitrogen	Clone B2D; RRID: AB_2784670
anti-mouse Tbet	BioLegend	Clone 4B10; RRID: AB_2561761
anti-mouse CXCR3	BioLegend	Clone CXCR3-173; RRID: AB_2566563
anti-mouse CXCR3	BioXCell	Clone CXCR3-173; RRID: AB_2687730
anti-mouse anti-CD3	DAKO	Clone F7.2.38; RRID: AB_579616
anti-mouse anti-Foxp3	Cell Signaling Technology	clone D6O8R; RRID: AB_2797974
anti-mouse anti-F4/80	Bio-Rad Laboratories	clone CI:A3-1; RRID: AB_1122716
anti-mouse anti-F4/80	Biolegend	Clone BM8; RRID: AB_893478
secondary Alexa Fluor® 488 - conjugated goat anti-rabbit	ThermoFisher Scientific	RRID: AB_2633280
Alexa Fluor® 647-conjugated goat anti-rat	ThermoFisher Scientific	RRID: AB_141778
secondary goat anti-mouse	Jackson Immunoresearch, West Grove, PA, USA	#115-065-068; RRID: AB_2338563
streptavidin-R-phycoerythrin	MossBio, Pasadena, MD, USA	RRID: AB_2337240
Bacterial and virus strains		
Helicobacter pylori strain PMSS1	Adrian Lee, Syndey, Australia	Lee et al., 1997
M. bovis BCG 1721	Peter Sander, UZH	N/A
Biological samples		
BCG-specific purified protein derivate (PPD)	Statens Serum Institut	N/A
Middlebrook 7H11 Agar	Millipore	M0428
Precision Plus qPCR Master Mix	Primer Design	N/A
Chemicals, peptides, and recombinant proteins		
brefeldin A	eBioscience	Catalog No. B7450
ionomycin	eBioscience	N/A
GolgiStop solution	BD Biosciences	554715
type IV collagenase	Sigma-Aldrich	C4-BIOC
metronidazole	Sigma-Aldrich	M1547
tetracycline hydrochloride	Sigma-Aldrich	CAS 64-75-5
bismuth subcitrate potassium	Selleckchem	Catalog No S4093
DNase I	Sigma-Aldrich	EN0521
Critical commercial assays		
Foxp3/Transcription Factor Staining Buffer Set	eBioscience	Catalog No. 50-112-8857
Cytofix/Cytoperm Fixation/Permeabilization Solution Kit	BD Biosciences	Catalog No. 554715

(*Continued on next page*)

Continued

REAGENT or RESOURCE	SOURCE	IDENTIFIER
NucleoSpin Tissue kit	Macherey-Nagel	REF 740952.50
Hprt TaqMan gene expression assay	Applied Biosystems	Mm03024075_m1
Tnf TaqMan gene expression assay	Applied Biosystems	Mm00443258_m1
Il12a TaqMan gene expression assay	Applied Biosystems	Mm00434169_m1
Csf2 TaqMan gene expression assay	Applied Biosystems	Mm01290062_m1
Cxcl9 TaqMan gene expression assay	Applied Biosystems	Mm00434946_m1
Cxcl10 TaqMan gene expression assay	Applied Biosystems	Mm00445235_m1
Il17a TaqMan gene expression assay	Applied Biosystems	Mm00439618_m1
Ifng TaqMan gene expression assay	Applied Biosystems	Mm01168134_m1
Experimental models: Organisms/strains		
C57BL/6	Janvier	N/A
Oligonucleotides		
M. bovis forward: 5′-TACGCTCG CGTTCGTGGT-3′	ThermoFisher Scientific	N/A
M. bovis reverse: 5′-GAT GAG TAT TAC CAG GCC GAC-3′	ThermoFisher Scientific	N/A
M. bovis probe: 5′-FAM-TCC GGG CGG CTG GGT GAT GTG-MGB-3′	ThermoFisher Scientific	N/A

RESOURCE AVAILABILITY

Lead contact

Further information and requests for resources and reagents should be directed to and will be fulfilled by the lead contact, Prof. Anne Müller (mueller@imcr.uzh.ch).

Materials availability

Requests for resources and reagents are available from the lead contact upon reasonable request.

Data and code availability

- All data reported in this paper will be shared by the lead contact upon request.
- This paper does not report original code.
- Any additional information required to reanalyze the data reported in this paper is available from the lead contact upon request.

EXPERIMENTAL MODEL AND SUBJECT DETAILS

Mouse experimentation

C57BL/6 mice were purchased from Janvier, and bred and maintained under specific pathogen-free conditions in accredited animal facilities at the University of Zurich. Mice were housed in groups of up to five mice in individually ventilated cages with access to water and chow ad libitum. Mixed gender groups were included in experiments at 6–7 weeks of age, and randomly assigned to experimental groups. All animal experimentation was reviewed and approved by the Zurich Cantonal Veterinary Office, which is the relevant body regulating animal work at the University of Zurich (licences ZH140/2017, ZH212/2018, ZH021/2020 and ZH086/2020 and their amendments) and adheres to the rules and regulations of the Swiss National Veterinary Office.

The *H. pylori* strain used in this study, PMSS1, is a clinical isolate of a patient with duodenal ulcer and the parental strain of the mouse-derivative Sydney strain 1 (SS1) (Arnold et al., 2011b) and was originally obtained from Adrian Lee, Univ. of New South Wales, Sydney, Australia. *H. pylori* was grown on horse blood agar plates and in liquid culture as described previously (Arnold et al., 2011b). Cultures were routinely assessed by light microscopy for contamination, morphology, and motility. Mice were infected orally on two consecutive days with 10^8 CFU H. pylori PMSS1 at > 6 weeks of age. For *M. bovis* BCG infection, we applied 5×10^6 CFU *M. bovis* BCG 1721, a derivative of *M. bovis* BCG Pasteur, either intraperitoneally, or intranasally under isofluorane anaesthesia. Bacterial stocks were kindly provided by Peter Sander, Institute of Medical Microbiology, University of Zurich. To assess BCG colonization, lungs, stomachs, spleens and livers were homogenized in a mini-bead beater (FastPrep-24 MP Biomedicals) for 1 min at 6.5 m/s

in pre-filled 2 mL tubes containing 1.5 mm zirconium beads (Benchmark) and 1 mL of PBS. Dilutions of tissue homogenates were plated onto Middlebrook 7H11 agar containing 10% OADC supplement (BD Biosciences) and 0.5% Tween 80. Plates were incubated at 37°C for 3–4 weeks and the number of BCG colonies (CFU) counted. *M. bovis* DNA was quantified by qPCR using *M. bovis*-specific primers; to this end, genomic DNA was extracted using NucleoSpin Tissue kit (Macherey-Nagel) following the manufacturer's instructions and subjected to qPCR using the Precision Plus qPCR Master Mix (Primer Design), and 100 μM TaqMan primers (forward: 5′-TAC GCT CGC GTT CGT GGT-3, reverse: 5′-GAT GAG TAT TAC CAG GCC GAC-3′, probe: 5′-FAM-TCC GGG CGG CTG GGT GAT GTG-MGB-3′, ThermoFisher Scientific) (Lesellier et al., 2019). A standard curve was generated using DNA isolated from *M. bovis* BCG. Antibiotic eradication therapy was achieved by daily intragastric administration (250 μL for 10 days) of 4.5 mg/mL metronidazole, 10 mg/mL tetracycline hydrochloride (both Sigma- Aldrich, Germany) and 1.2 mg/mL bismuth subcitrate potassium (Selleckchem, USA). For *M. bovis*-specific immunization, 1.7×10^6 CFU of *M. bovis* BCG were subcutaneously injected into one flank of isoflurane-anesthetized mice. The CXCR3 blocking antibody (clone: CXCR3-173) was purchased from BioXCell (West Lebanon, NH) and administered twice a week intraperitoneally (250 μg per dose). Polyclonal Armenian hamster IgG (BioXCell) was used as isotype control.

METHOD DETAILS

Assessment of gastric histopathology

For histopathological analysis, one third of each stomach was fixed in 10% neutral-buffered formalin prior to paraffin embedding and stained with H&E, Alcian Blue and for immunohistochemistry with an anti-mouse Ki67 antibody (clone B56, BD Bioscience). One to three longitudinal sections per mouse spanning the length of the stomach from the forestomach/corpus junction to the antrum/duodenum junction were scored with regard to four histopathological parameters (chronic inflammation, gastric atrophy, intestinal metaplasia, mucus pit cell/epithelial hyperplasia), based on the features described in the updated Sydney classification (Chen et al., 1999). We attributed scores on a scale of 0–6 as proposed by Chen et al. (Chen et al., 1999). Specifically, the definition of scores was as follows for the four parameters evaluated. Chronic inflammation: 0, none; 1, some infiltrates; 2, mild (few aggregates in submucosa and mucosa); 3, moderate (several aggregates in submucosa and mucosa); 4, marked (many big aggregates in submucosa and mucosa); 5, nearly the entire mucosa contains a dense infiltrate; 6, entire mucosa contains a dense infiltrate. Atrophy: 0, none; 1, foci where a few gastric glands are lost or replaced; 2, small areas in which gastric glands have disappeared or been replaced; 3, <25% of gastric glands lost or replaced; 4, 25–50% of gastric glands lost or replaced; 5, >50% of gastric glands lost or replaced; 6, only a few small areas of gastric differentiated glands remaining. Intestinal metaplasia: 0, none; 1, only one crypt replaced by intestinal epithelium (i.e.); 2, one focal area (1–4 crypts) replaced; 3, two separate foci with metaplasia; 4, multiple foci; 5, >50% of gastric epithelium replaced by i.e.; 6, only a few small areas of gastric epithelium are not replaced by i.e. Hyperplasia: 0, none; 1, single glands (next to infiltrate); 2, one focal area/1–4 crypts (mild); 3; 1–3 foci; 4, multiple foci; 5, >50% of glands affected; 6, only few small non-hyperplasic areas.

Leukocyte isolation

For gastric lamina propria leukocyte isolation, stomachs were opened longitudinally, washed and cut into pieces. Pieces were incubated in Hanks' balanced salt solution with 10% FCS and 5 mM EDTA at 37°C to remove epithelial cells. Tissue was digested at 37°C for 50 min in a shaking incubator with 15 mM HEPES, 500 U/mL of type IV collagenase (Sigma-Aldrich) and 0.05 mg mL^{-1} DNase I in supplemented RPMI-1640 medium. Cells were then layered onto a 40/80% Percoll gradient, centrifuged, and the interface was washed in PBS with 0.5% BSA. Liver cell suspensions were prepared by chopping the liver into pieces and digestion at 37°C for 45 min in a shaking incubator with 500 U/mL of type IV collagenase (Sigma-Aldrich) and 0.05 mg mL−1 DNase I in supplemented RPMI-1640 medium. Cells were layered onto a 40/75% Percoll gradient, centrifuged and the interface was washed in PBS with 0.5% BSA.

Flow cytometry, T-cell re-stimulation and cell sorting

Cells were stained with a fixable viability dye and a combination of the following antibodies: anti-mouse CD45 (clone 30-F11), CD4 (RM4-5), CD8 (53-6.7), TCRβ (H57-597), Neuropilin-1 (3×10^{12}) or an IgG isotype control (all from BioLegend). Fc block (anti-CD16/CD32, Affymetrix) was included to minimize nonspecific antibody binding. For intracellular cytokine staining, the cells were incubated at 37°C for 3.5 h in complete IMDM medium containing 0.1 μM phorbol 12-myristate 13-acetate and 1 μM ionomycin with 1:1,000 brefeldin A (eBioscience) and GolgiStop solutions (BD Biosciences) at 37°C in a humidified incubator with 5% CO2. BCG-infected cell suspensions were re-stimulated re-stimulated *in vitro* with 5 μg/mL BCG-specific purified protein derivate (PPD) from Statens Serum Institut (Copenhagen, Denmark). Following surface staining, cells were fixed and permeabilized with the Cytofix/Cytoperm Fixation/Permeabilization Solution Kit (BD Biosciences) according to the manufacturer's instructions. Cells were stained for 50 min with antibodies to IL-17A (TC11-18H10.1), IFN-γ (XMG1.2) and TNF-α (MP6-XT22). For the intranuclear staining of transcription factors, cells were fixed and permeablized with the Foxp3/Transcription Factor Staining Buffer Set (eBioscience) after surface staining according to the manufacturer's instructions. Cells were stained for 50 min with antibodies to FoxP3 (FJK-16s), RORγt (B2D) from Invitrogen, and Tbet (4B10) from BioLegend. Samples were acquired on a LSRII Fortessa (BD Biosciences) and analyzed using Flowjo software.

Multiplex serology

Serum antibodies to selected *H. pylori* proteins were quantified using Multiplex Serology (Michel et al., 2009; Waterboer et al., 2005). Briefly, *H. pylori* proteins were expressed as recombinant GST-fusion proteins and coupled to spectrally distinguishable glutathione-casein coated polystyrene beads (SeroMap, Luminex Corp., Austin, TX, USA). The beads were combined into a single mix and added to each of the pre-diluted mouse sera (1:100). Serum antibodies were subsequently quantified using a secondary goat anti-mouse antibody (1:1000, #115-065-068, Jackson Immunoresearch, West Grove, PA, USA) and streptavidin-R-phycoerythrin (1:750, Moss-Bio, Pasadena, MD, USA). For each bead, the respective antigen and bound serum antibodies were determined using a Luminex 200 instrument (Luminex Corp., Austin, TX, USA). At least 100 beads were analyzed to generate the raw median fluorescence intensity (MFI) per serum and antigen. Unspecific background and serum-specific GST background were subtracted from the raw values to obtain final MFI values.

Quantitative PCR

RNA was isolated from scraped gastric mucosa or from liver slices using the RNeasy Mini kit (QIAGEN) according to the manufacturer's instructions. Complementary DNA synthesis was performed using Superscript III reverse transcriptase (QIAGEN). Quantitative PCR reactions for the candidate genes were performed using TaqMan gene expression assays (Hprt Mm03024075_m1, Ifng Mm01168134_m1, Tnf Mm00443258_m1, Il12a Mm00434169_m1, Csf2 Mm01290062_m1, Cxcl9 Mm00434946_m1, Cxcl10 Mm00445235_m1, Il17a Mm00439618_m1, Applied Biosystems). Complementary DNA samples were analyzed in duplicate using a Light Cycler 480 detection system (Roche) and gene expression levels for each sample were normalized to HPRT expression. Mean relative gene expression was determined, and the differences were calculated using the 2ΔC(t) method.

Immunofluorescence and confocal microscopy

Paraffin-embedded tissue sections were deparaffinized and rehydrated with graded ethanol dilutions. After antigen retrieval in a pressure cooker using sodium citrate buffer (10 mM, pH 6.0), the non-specific binding was prevented by preincubation of the tissue samples with a blocking buffer (containing human immunoglobulins, normal goat serum, and 7.5% BSA in PBS) at room temperature (RT) for 1 h. Indirect immunofluorescence staining was performed by incubating the paraffin sections overnight at 4°C with mouse monoclonal anti-CD3 antibody (1:20; clone F7.2.38; DAKO, distributed by Agilent Technologies AG, Basel Switzerland), rabbit monoclonal anti-Foxp3 antibody (1:100; clone D6O8R; Cell Signaling Technology, distributed by BioConcept, Allschwil, Switzerland), and rat monoclonal anti-F4/80 (1:50; clone CI:A3-1; Bio-Rad Laboratories AG, Hercules, USA) and/or rat monoclonal anti-F4/80 (1:50; clone BM8; Biolegend, Amsterdam, Netherland). Thereafter, secondary Alexa Fluor 488 - conjugated goat anti-rabbit (1:400), Alexa Fluor 545-conjugated goat anti-mouse (1:400), and Alexa Fluor 647-conjugated goat anti-rat antibodies (ThermoFisher Scientific, Reinach, Switzerland) were applied, and tissue samples incubated at RT for 1 h, and stained with Hoechst 33,342 solution (5 μM) for additional 10 min. Samples were washed and mounted in Prolong Gold mounting medium and image acquisition was performed using confocal laser scanning microscopy LSM 810 (Carl Zeiss Micro Imaging, Jena, Germany) with a 63× or 40×/1.40 Oil DIC objectives and analyzed with IMARIS software (Bitplane AG, Zurich, Switzerland). For better visualization, the gamma correction function together with min/max thresholds of Imaris software was used to optimize the image display by intensifying the values for grey (F4/80), green (Foxp3), and red (CD3) colours. For quantitative analysis, Foxp3+ and CD3+ infiltrating cells were counted in 10 high-power fields (hpf) of highest activity using an automated slide scanner (3DHISTECH slide scanner, Quant Center software, using Cell Count module).

TCGA data analysis and annotation of *H. pylori* and Mtb status

TCGA stomach adenocarcinoma mutation, copy number data and gene count data were downloaded with the R package TCGAbiolinks (Colaprico et al., 2016). Molecular subtyping was performed based on a previous publication (Bass et al., 2014). The Oncoprint-like plot was generated using the R package ComplexHeatmap (Gu et al., 2016). Damaging mutations were defined by having a ''deleterious'' annotation from SIFT and ''damaging'' annotation from PolyPhen. To annotate stomach adenocarcinoma (STAD) samples from TCGA with *H. pylori* and Mtb status, we acquired whole-genome (WGS), whole-exome (WXS), and transcriptome (RNA-seq) sequencing data from TCGA via the application programming interface (API) of the National Cancer Institute's (NCI) Genomic Data Commons (GDC). Mtb and *H. pylori* status was determined using data from The Cancer Microbiome Atlas (TCMA)'' as described (Dohlman et al., 2021). Briefly, raw sequencing data in bam format were screened for *H. pylori* and Mtb using the PathSeq pipeline (Kostic et al., 2011), which is available through the Broad Institute's Genome Analysis Tooklit (GATK v4.0.3). Mtb counts were determined by mapping TCMA sequencing reads to the Mtb genome (GenBank CP002095.1). The PathSeq analysis was performed using prebuilt human and microbial reference genomes from the PathSeq resource bundle, available through the Broad Institute's Genome Sequence Archive (GSA) FTP server. All sequencing data were analyzed using a local high-performance computing cluster. Reads per million (RPM) was calculated by dividing the number of reads aligning to each species by the total number of sequencing reads from each corresponding experiment. *H. pylori* status of a sample was determined by having at least 1 aligned read in either WGS or RNAseq from the tumor tissue or either WGS, WES, or RNAseq from normal adjacent tissue; Mtb status of a sample was determined by having at least 0.01 reads per million unambiguously aligned in either WGS or WES from tumor as well as adjacent tissue. Tumor infiltrating cells were estimated with CIBRSORT running in absolute mode (Newman et al., 2015). Differential gene expression was performed with limma voom (Law et al., 2014).

QUANTIFICATION AND STATISTICAL ANALYSIS

Statistical analysis was performed with Prism 6.0 (GraphPad Software). The nonparametric Mann-Whitney U test was used for all direct statistical comparisons between two groups; the Kruskal-Wallis test was used for comparisons of more than two groups, followed by Dunn's post-hoc test. Differences were considered statistically significant when $p < 0.05$. * indicates $p < 0.05$, **$p < 0.01$, ***$p < 0.001$, ****$p < 0.0001$.